REVIEW

Dark stars: a review

IOP Publishing Reports on Progress in Physics
Rep. Prog. Phys. **79** (2016) 066902 (24pp) doi:10.1088/0034-4885/79/6/066902

Review

Dark stars: a review

Katherine Freese[1,2,3], Tanja Rindler-Daller[3,4], Douglas Spolyar[2] and Monica Valluri[5]

[1] Nordita (Nordic Institute for Theoretical Physics), KTH Royal Institute of Technology and Stockholm University, Roslagstullsbacken 23, SE-106 91 Stockholm, Sweden
[2] The Oskar Klein Center for Cosmoparticle Physics, AlbaNova University Center, University of Stockholm, 10691 Stockholm, Sweden
[3] Department of Physics and Michigan Center for Theoretical Physics, University of Michigan, 450 Church St., Ann Arbor, MI 48109, USA
[4] Institute for Astrophysics, Universitätssternwarte Wien, University of Vienna, Türkenschanzstr. 17, A-1180 Wien, Austria
[5] Department of Astronomy, University of Michigan, 1085 South University Ave., Ann Arbor, MI 48109, USA

E-mail: daller@umich.edu

Received 16 October 2014, revised 31 January 2016
Accepted for publication 9 March 2016
Published 23 May 2016

Abstract

Dark stars are stellar objects made (almost entirely) of hydrogen and helium, but powered by the heat from dark matter annihilation, rather than by fusion. They are in hydrostatic and thermal equilibrium, but with an unusual power source. Weakly interacting massive particles (WIMPs), among the best candidates for dark matter, can be their own antimatter and can annihilate inside the star, thereby providing a heat source. Although dark matter constitutes only $\lesssim$0.1% of the stellar mass, this amount is sufficient to power the star for millions to billions of years. Thus, the first phase of stellar evolution in the history of the Universe may have been dark stars. We review how dark stars come into existence, how they grow as long as dark matter fuel persists, and their stellar structure and evolution. The studies were done in two different ways, first assuming polytropic interiors and more recently using the MESA stellar evolution code; the basic results are the same. Dark stars are giant, puffy ($\sim$10 AU) and cool (surface temperatures $\sim$10 000 K) objects. We follow the evolution of dark stars from their inception at $\sim 1 M_\odot$ as they accrete mass from their surroundings to become supermassive stars, some even reaching masses $>10^6 M_\odot$ and luminosities $>10^{10} L_\odot$, making them detectable with the upcoming James Webb Space Telescope. Once the dark matter runs out and the dark star dies, it may collapse to a black hole; thus dark stars may provide seeds for the supermassive black holes observed throughout the Universe and at early times. Other sites for dark star formation may exist in the Universe today in regions of high dark matter density such as the centers of galaxies. The current review briefly discusses dark stars existing today, but focuses on the early generation of dark stars.

Keywords: astroparticle physics, dark matter, first stars, cosmology

(Some figures may appear in colour only in the online journal)

1. Introduction

Dark stars (DSs) are stellar objects powered by the heat from dark matter (DM) annihilation. We will focus on the DSs that may have been the first stars to form in the history of the Universe, and briefly discuss DSs that may exist today.

The first stars formed when the Universe was roughly 200 million years old, at redshifts $z \sim 10$–50. We will show that

these first stars, which form in a dark matter rich environment, may have been dark stars, powered by dark matter heating rather than by fusion for millions to billions of years. Only after the dark matter fuel was exhausted could fusion take over as the power source inside stars[6].

Weakly interacting massive particles (WIMPs) are thought to be among the best motivated dark matter candidates. Many WIMP candidates are their own antiparticles, and if they are initially in thermal equilibrium in the early Universe, they annihilate with one another so that a predictable number of them remain today. Once the annihilation rate drops below the Hubble expansion rate, the abundance of WIMPs freezes out. The relic density of these particles is approximately [1, 2]

$$\Omega_\chi h^2 \simeq \frac{3 \times 10^{-27} \mathrm{cm}^3\,\mathrm{s}^{-1}}{\langle \sigma v \rangle}, \qquad (1)$$

where Ω_χ is the fraction of the energy density in the Universe today in the form of WIMPs and h is the Hubble constant in units of 100 km s^{-1} Mpc^{-1}. With the simple assumption that the annihilation cross section $\langle \sigma v \rangle$ is determined by weak interaction strength, then WIMPs automatically produce roughly the correct dark matter density today, ∼25% of the total content of the Universe [3, 4]. This coincidence is known as 'the WIMP miracle' and is the reason why WIMPs are taken so seriously as DM candidates. The Universe as a whole consists of roughly 5% baryonic material, 25% dark matter, and 70% dark energy[7]. There is a second reason for the interest in WIMPs as dark matter candidates: WIMPs automatically exist in particle theories designed to solve problems that have nothing to do with dark matter. Supersymmetric (SUSY) extensions of the standard model of particle physics predict the existence of new partners for every particle in the standard model and, given R-parity, the lightest of these would be dark matter candidates. In particular, an excellent WIMP candidate is the lightest neutralino in the minimal supersymmetric standard model. Models of universal extra dimensions may also have WIMP dark matter candidates in the theories (e.g. Kaluza–Klein particles)[8].

The same annihilation process that took place throughout the early Universe continues in those locations where the dark matter density is sufficiently high for WIMPs to encounter one another and annihilate. The first stars to form in the Universe are a natural place to look for significant amounts of dark matter annihilation, because they formed 'at the right place and the right time': they formed early (when the Universe was still substantially denser than it is today), and at the high density centers of dark matter halos.

The formation of large-scale structures in the Universe—the galaxies and galaxy clusters—took place via a process known as hierarchical clustering. As the dominant component of the mass in the Universe, dark matter drove the dynamics of this formation of structure. Small (sub-Earth-sized) clumps formed first; then these merged together to make larger structures; and eventually these merged yet further to produce the galaxies and clusters we see today. These clumps of various sizes, known as 'dark matter halos', are spheroidal (prolate or triaxial) objects containing 85% dark matter and 15% atomic matter. The remainder of the Universe, the dark energy, does not respond to the attractive force of gravity and instead produces an accelerated expansion of the Universe; dark energy played no role in the formation of the first stars.

At the time of the formation of the first stars, the atomic matter in the Universe consisted only of hydrogen, helium, and a smattering of heavier elements (Li, B, Be)—the products of primordial nucleosynthesis that took place three minutes after the big bang. All the other more complex elements were only able to form later, as the products of fusion in stars.

Once dark matter halos about a million times as massive as the Sun ($10^6 M_\odot$), known as 'minihalos'[9], were able to form, the conditions were ripe for the formation of the first stars, known as Population III stars. The virial temperatures of minihalos led to molecular hydrogen cooling that allowed a protostellar cloud to start to collapse towards the center of the halo. Reviews of the standard picture of the formation of the first stars, without taking into account the role of dark matter, can be found in [6–11].

It was the idea of some of the authors of this review to ask, what is the effect of the DM on these first stars? We studied the behavior of WIMPs in the first stars, and found that they can radically alter the stars' evolution [12]. The annihilation products of the dark matter inside the star can be trapped and deposit enough energy to heat the proto-star and prevent it from further collapse. A new stellar phase results, a 'dark star', powered by DM annihilation as long as there is DM fuel, for possibly millions to billions of years. The DM—while only a negligible fraction of the star's mass—provides the key power source for the star through DM heating. Note that the term 'dark' refers to the power source, not the material or the appearance of the star. Early DSs are stars made primarily of hydrogen and helium with a smattering of dark matter; typically less than 0.1% of the mass consists of DM. Yet, DSs shine due to DM heating.

In the past few years, we have done extensive studies of the stellar structure and evolution of DSs. Dark stars are born with masses $\sim 1 M_\odot$ and then grow to much larger masses. They are giant, puffy (10 AU), and cool (surface temperatures ∼10 000 K) objects [13]. Since the DSs reside in a large reservoir of baryons (15% of the total halo mass), the baryons can start to accrete onto the DSs. Our work [13–16] followed the evolution of DSs from their inception at $\sim 1 M_\odot$, as they accreted mass from their surroundings to become supermassive stars, possibly as large as $10^7 M_\odot$.

We now have used two different approaches in studying the evolution of dark stars. In our initial studies, we assumed that the star can be described as a polytrope with the relationship

[6] The largest supermassive dark stars may bypass fusion altogether and collapse directly to black holes.

[7] There is some disagreement between the best fit values of the PLANCK and WMAP satellites [3, 4], but the numbers we quote here are roughly correct [3, 4].

[8] DM is not limited to self-conjugate Majorana states, but these are traditionally the most studied possibilities.

[9] Minihalos are defined as halos with virial temperatures below about 10^4 K, where molecular cooling prevails over atomic cooling mechanisms. The mass range of minihalos depends on the redshift: their maximum mass lies between $1–2 \cdot 10^7 M_\odot$ in a redshift range of $z = 15–20$, see [5].

between pressure P and density ρ at a given radius determined by the polytropic index n,

$$P = K\rho^{1+1/n}, \tag{2}$$

where the 'constant' K is determined, once we know the total mass and radius [17]. More recently, we have used MESA, a fully-fledged 1D stellar evolution code which allows us to solve the stellar structure equations self-consistently, without any *a priori* assumptions on the equation of state. Remarkably, our findings show that the previous results using polytropes roughly match (up to factors of 2) the more accurate results using MESA, though there are some differences in the details [16]. Now that we have the MESA code we can perform future studies of interesting effects like DS pulsations.

DSs are stable as long as there is DM to fuel them. Indeed, as long as there is a reservoir of DM to heat the DS, the star continues to grow. There are two main methods for sustaining DM fuel: (1) gravitational attraction of dark matter particles on a variety of orbits (extended adiabatic contraction) and (2) capture by atomic nuclei due to elastic scattering. The key ingredient that allows DSs to grow so much larger than ordinary fusion-powered Population III stars is the fact that DSs are so much cooler. Fusion-powered Pop III stars have much larger surface temperatures in excess of 50 000 K. They produce ionizing photons that provide a variety of feedback mechanisms that cut off further accretion. In [18], it was estimated that the resultant Pop III stellar masses are $\sim 140 M_{\odot}$. DSs are very different from fusion-powered stars, and their cooler surface temperatures allow continued accretion of baryons all the way up to enormous stellar masses.

Supermassive DSs can in principle grow to any mass as long as the dark matter power persists—e.g. as large as $10^7 M_{\odot}$ with luminosities of $10^{11} L_{\odot}$. Thus, they should be observable with the James Webb Space Telescope (JWST), the successor to the Hubble Space Telescope, which is expected to be launched in 2018. It is an exciting prospect that an entirely new type of star may be discovered in these upcoming data.

Once DSs run out of dark matter fuel, they start to collapse and can become hot enough for fusion to begin. Supermassive DSs may even collapse directly to black holes. In either case, whether or not there is a brief period of fusion, the final end state of most DSs will be black holes with masses in excess of $10^4 M_{\odot}$. These black holes, that are the remnants of DSs, serve as seeds for the many supermassive black holes throughout the Universe, including those at the centers of galaxies and in AGNs in the early Universe. Some may also become intermediate-mass black holes which have been recently discovered, see [19, 20].

For a short list of papers by various other authors that have continued the work of [12] and explored the repercussions of DM heating in the first stars, see [21–28]. Their potential observability has been discussed in [15, 29, 30] (see section 6). The impact on reionization and the cosmic microwave background of populations of DSs below about 1000 $M_{\odot}$ have been studied in [31] and [32], leading to contraints on their life times and abundance (see section 9).

The investigation of the effect of DM on stars (in the present-day Universe) dates back to [33], which studied the impact of massive neutrinos on galaxies and stars. The first paper discussing DM annihilation in stars was by [34]. The first papers suggesting searches for annihilation products of WIMPs in the Sun were by [35]; and in the Earth by [36], as well as by [37]. Implications of annihilation for stellar evolution were first explored by [38] and [39]. References [34, 40, 41] first studied the effect of DM energy transport upon the Sun. There was a proposal to solve the solar neutrino problem [40, 41] by using 'cosmions', an idea no longer pursued. Our Sun is 24 000 light years away from the center of our Galaxy—too far away to be powered by DM annihilation, though experimenters are searching for the products (particularly neutrinos) of the annihilation of the small amounts of DM captured by the Sun, [42].

DM heating can also dramatically affect stars at the galactic center, where DM densities can be orders of magnitudes larger than found locally. [38, 43] were the first to carefully study the effects of dark matter on stars at the galactic center. More recently, the effect on today's stars has been re-examined under the assumption that DM is made of WIMPs [44–48] or within the hypothesis of inelastic dark matter [49]. [50] presented the darkstars code: a publicly available dark stellar evolution package. [44, 46] looked at DM heating in white dwarves, and neutron stars, at the galactic center and in globular clusters, often referred to as 'WIMP Burners'.

In this review, we will focus on the effect of DM on the first stars with a brief discussion of dark stars today in section 10. This same WIMP annihilation process that powers DSs is also the basis for DM indirect detection searches. Currently, there are several observations of excess γ-rays (particularly from the FERMI gamma-ray space telescope [51, 52]) that may point to a dark matter annihilation origin. Some have argued that excess positrons (seen in HEAT [53], PAMELA [54] and AMS [55, 56]) may also be due to DM annihilation, but some of us have found severe bounds on this interpretation [57]; see also [58]. The origin of the positron excess is likely some other astrophysical source.

The organization of this review is as follows: in section 2, we review the three criteria required for the initial formation of dark stars: high dark matter density inside the stars, the trapping of DM annihilation products inside the stars, and DM heating dominating over all other cooling and heating mechanisms inside the stars. In section 3, we discuss the accretion of mass onto the initial DSs, thereby building up their mass. Next we illustrate in section 4 the equilibrium structure of the DSs. We begin with the basic equations, and outline the polytropic approach and the MESA calculation. We discuss the energy sources, in turn dominated by DM annihilation due to adiabatically contracted DM, gravity, fusion, and finally captured DM. A key ingredient in DSs is the dark matter density, so we discuss the initial density profile, as well as the adiabatic contraction and capture that can bring more DM into the star. In section 5, we review the results of the stellar structure analysis, including figures showing our results: the luminosity evolution, the Hertzsprung–Russell diagram,

and the baryonic and DM density profiles inside DSs. We also here respond to a critique: we point out that we agree that the initial DSs are quite dense, beyond the resolution of any existing simulations of protostellar collapse. Then, in section 6 we show that JWST should be able to discover supermassive DSs (more massive than $\sim 10^5 M_\odot$). As shown in section 7, a new avenue of detectability would be stellar pulsations of DSs, some having periods in the observers' frame of the order of months. As discussed in section 8, the final end product of DSs will be black holes (BHs), including seeds for the supermassive BHs observed throughout the Universe and found even at early times. In addition, we discuss constraints on BHs with DM spikes around them residing within our Galaxy today, due to γ-rays detectable by FERMI. In section 9, we review previous work on the impact of DSs on the cosmic microwave and infrared backgrounds. A very brief review follows in section 10 on dark stars in the present Universe. Finally, we end with a conclusion in section 11.

2. Initial formation of dark stars: three criteria for dark matter heating

Dark stars are powered by WIMP annihilation. The WIMP annihilation rate is $n_\chi^2 \langle \sigma v \rangle$ where n_χ is the WIMP number density. We take the standard annihilation cross section (the value that produces the correct DM abundance in the Universe today)

$$\langle \sigma v \rangle = 3 \times 10^{-26}\,\mathrm{cm^3\,s^{-1}}. \tag{3}$$

Since the WIMP mass is converted to energy in the annihilation, WIMP annihilation produces energy at a rate per unit volume

$$\hat{Q}_{\rm DM} = n_\chi^2 \langle \sigma v \rangle m_\chi = \langle \sigma v \rangle \rho_\chi^2 / m_\chi, \tag{4}$$

where ρ_χ is the WIMP mass density. As our canonical case we take $m_\chi = 100$ GeV, but we also studied a wide range of possible WIMP masses in the range $m_\chi = 10$ GeV–1 TeV. Since the DM heating scales as $\hat{Q}_{\rm DM} \propto \langle \sigma v \rangle / m_\chi$, by studying a variety of WIMP masses we are effectively studying a comparable range of annihilation cross sections. The existence of dark stars is essentially insensitive to either the WIMP mass or the cross-section, within many orders of magnitude: for smaller annihilation cross-sections (or equivalently larger WIMP masses), the initial DS mass would be slightly smaller, but would quickly grow to look similar to the DS in the case of higher cross-section or lighter WIMP mass.

Spolyar *et al* [12] (hereafter paper I) outlined the three key ingredients for DSs: (1) high dark matter densities, (2) the annihilation products become trapped inside the star, and (3) DM heating wins over other cooling or heating mechanisms. These same ingredients are required throughout the evolution of the DSs, whether during its formation or during its main evolutionary phase.

First criterion: high dark matter density inside the star. One can see from equation (4) that the DM annihilation rate scales as WIMP density squared, because two WIMPs must find each other to annihilate. Thus, the annihilation is significant wherever the density is high enough. Dark matter annihilation is a powerful energy source in these first stars because the dark matter density is high inside the early DSs. First, DM densities in the early Universe were higher by $(1+z)^3$ at redshift z. Second, the first stars form exactly in the centers of DM halos where the densities are high. (Most of today's stars, by contrast, are scattered throughout the disk of the galaxy where the DM density is low; few are situated at the Galactic Center where the DM density is high). Third, a further DM enhancement takes place in the center of the halo: as the protostar forms, it deepens the potential well at the center and pulls in more DM as well. As discussed in further detail below, we have computed this enhancement in several ways. Initially, in paper I we used the simplistic Blumenthal method of adiabatic contraction (see also [59]), and found the following approximation on how the DM density follows the (baryonic) gas density n_h, due to adiabatic contraction,

$$\frac{\rho_\chi}{\mathrm{GeV cm^{-3}}} \simeq 5 \left(\frac{n_h}{\mathrm{cm^{-3}}} \right)^{0.81}. \tag{5}$$

We then confirmed that our results were correct to within a factor of two when we performed an exact calculation in [60]. We took the gas profile which was calculated in the first-star-simulation of [10]; it is this profile which enters as n_h in equation (5).

Inserting this result of equation (5) into equation (4), we find that WIMP annihilation produces energy at a rate per unit volume roughly given by

$$\hat{Q}_{\rm DM} \simeq 10^{-29} \frac{\mathrm{erg}}{\mathrm{cm^3\,s^{-1}}} \frac{\langle \sigma v \rangle}{(3 \times 10^{-26}\,\mathrm{cm^3\,s^{-1}})} \left(\frac{n_h}{\mathrm{cm^{-3}}} \right)^{1.6} \left(\frac{100\ \mathrm{GeV}}{m_\chi} \right). \tag{6}$$

In performing our subsequent calculations, we do not use this approximation but instead use adiabatic contraction to follow the DM density more accurately. Fourth, at later stages, we also consider an additional source of DM in the star due to capture of dark matter by atomic nuclei. As discussed further below, as DM from the halo passes through the DS, some WIMPs scatter off nuclei and are captured into the DS, see [22, 61].

We assume for our standard case that the DM density inside the $10^6 M_\odot$ DM halo initially has an NFW profile [62]. However, our results do not depend on this choice of initial DM profile. Indeed, for comparison we even took the extreme case of a flat Burkert profile at the center of the halo, which is not thought to be realistic, and still found a sufficiently enhanced DM density to produce a DS; see [60]. We also note that recent simulations in [63] indicate that observations of cored profiles in some galaxies today could still be consistent with cuspy early halos: supernovae and other feedback mechanisms could be responsible for reducing the central densities of halos today, while early halos (such as those where DSs formed) could have had NFW profiles.

Second criterion: dark matter annihilation products become trapped inside the star. In the early stages of first star

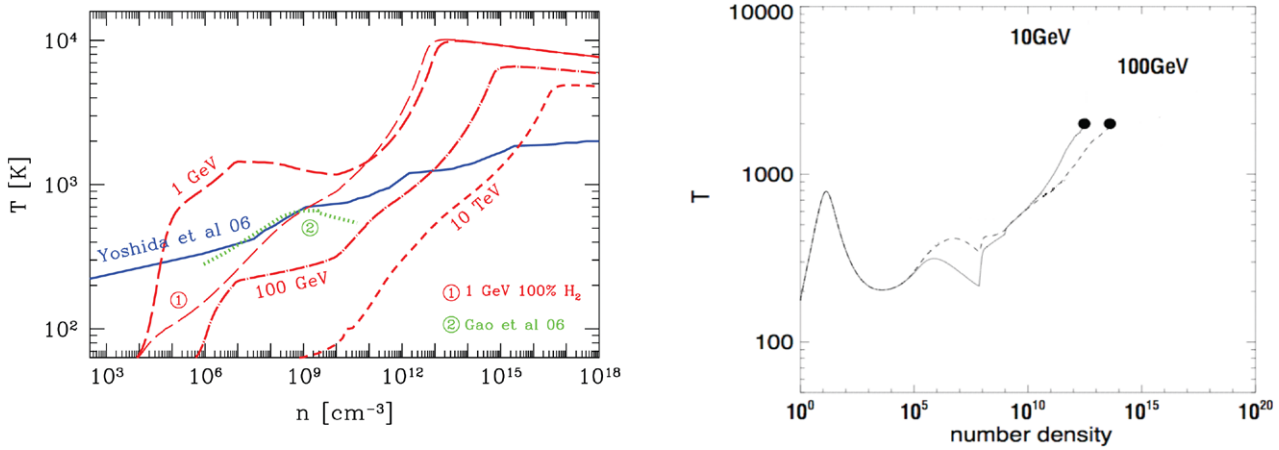

Figure 1. Temperature (in degrees K) as a function of hydrogen density (in cm^{-3}) for the first protostars, with DM annihilation included. Moving to the right in the figures corresponds to moving forward in time. *Left-hand plot:* Critical temperature lines above which DM heating dominates over cooling in the core. The solid (blue) and dotted (green) lines show the protostellar gas evolution from first-star simulations of [11, 71]. The dashed (red) lines mark critical temperature lines for different DM particle masses, (i) 1 GeV with H_2 density from simulations, (ii) 1 GeV assuming 100 % H_2 cooling, (iii) 100 GeV, (iv) 10 TeV. At the crossing point of the solid (blue) or dotted (green) with the dashed (red) lines, DM heating dominates over cooling in the core's evolution. (Figure reproduced with permission from [12]). *Right-hand plot:* More accurate calculation using a first-star simulation code, for two different DM particle masses (10 GeV and 100 GeV). Once the 'dots' are reached, DM annihilation dominates over H_2 cooling, and a proto-DS is created. The conditions at that point are the starting values for the stellar evolution calculation. (Figure courtesy of Yoshida, see [72]). The results in both figures are consistent with each other.

formation, when the gas density is low, most of the annihilation energy is radiated away [64]. However, as the gas collapses and its density increases, a substantial fraction f_Q of the annihilation energy is deposited into the gas, heating it up at a rate $f_Q \hat{Q}_{\mathrm{DM}}$ per unit volume. The annihilation products and their energy spectrum depend on the WIMP model: for neutralino DM, the annihilation products typically are 1/3 neutrinos, 1/3 photons and 1/3 charged stable particles (electrons and positrons). While neutrinos escape from the cloud without depositing an appreciable amount of energy, the rest can transmit energy to the core. Thus, we can take

$$f_Q \simeq 2/3\,. \tag{7}$$

For a 100 GeV WIMP, the energy due to electrons and photons is trapped inside the star once the hydrogen density exceeds $\sim 10^{13}$ cm^{-3}. Thus, around 2/3 of the annihilation energy is then trapped inside the collapsing gas, thermalizes with it, and provides a heat source for the resulting dark star.

In our original work, we actually computed the energy deposition more precisely, as we discuss in the next few paragraphs. The quantity f_Q scales linearly with the gas density and depends on the relative number of the various annihilation products and their energy spectrum. The energy spectrum of photons and electrons depends to some extent on the exact annihilation channels. As a typical case, we considered spectra produced in Pythia simulations of 500 GeV neutralino annihilation [65, 66]. Other spectral shapes will change the precise values of our results but not the overall effect.

Electrons below a critical energy $E_c \approx 280$ MeV in hydrogen lose energy predominantly by ionization. Higher energy electrons do so by emission of bremsstrahlung photons. As these bremsstrahlung photons pass near gas nuclei, they create electrons and positrons, which in turn may generate other bremsstrahlung photons. Thus starts a sequence of photon, electron, and positron conversions: an electromagnetic (EM) cascade. While photons above ≈100 MeV also initiate an EM cascade, lower energy photons transfer most of their energy to electrons in the gas (Compton scattering).

We approximated the energy loss of electrons via ionization with 4.41 MeV/E (g cm^{-2})$^{-1}$. For EM cascades, we assumed a gamma distribution for the mean longitudinal profile. Thus, the fraction of energy lost in traversing a thickness X of gas equals $\gamma(a, bX/X_0)/\Gamma(a)$, where $\gamma(x, y)$ is the incomplete gamma function, $X_0 = 63\,\mathrm{g\ cm}^{-2}$ is the radiation length in hydrogen, $a = 1 + b[\ln(E/E_c) - 0.5]$, and $b = 0.5$ [67]. We estimate the core thickness as $X = 1.2 m_p n r_0$. Here m_p is the proton mass, r_0 is the core radius, and the factor of 1.2 is appropriate for a uniform sphere. We modeled the fraction of energy loss of photons by converting each photon to an electron of the same energy after one photon attenuation length. The latter is computed from formulas in [68], interpolated to produce the hydrogen curve in [67], figure 27.16. There is no question that a significant fraction of the annihilation energy gets trapped inside the star, once its hydrogen density is high enough. Indeed, we demanded ~ 80 radiation lengths, which is far more demanding than necessary to trap the energy. We then compared the DM heating resulting from these studies with the stellar cooling.

Third criterion: DM heating is the dominant heating/cooling mechanism in the star. We find that, for a WIMP mass of $m_\chi = 100$ GeV (1 GeV), a crucial transition takes place when the gas density reaches $n > 10^{13}\,\mathrm{cm}^{-3}$ ($n > 10^{9}\,\mathrm{cm}^{-3}$). Above this density, DM heating dominates over all relevant cooling mechanisms, the most important being H_2 cooling [69].

Figure 1 shows evolutionary tracks of the protostar in the temperature-density phase plane with DM heating included [70], for two DM particle masses (10 GeV and 100 GeV). Moving to the right on this plot is equivalent to moving

forward in time. Once the black dots are reached, DM heating dominates over cooling inside the star, and the proto-DS phase begins. The size of the core at this point is $\sim$ 17 AU and its mass is $\sim 0.6 M_\odot$ for 100 GeV mass WIMPs. The proto-DS keeps collapsing until equilibrium is reached[10]. Eventually, above a certain baryonic density threshold, which depends on the WIMP mass, the annihilation products that remain trapped in the star thermalize and provide a heat source for hydrostatic and thermal equilibrium: a new type of object is created, a DS supported by DM annihilation rather than fusion.

One can see the power of DM heating: although the DM constitutes a tiny fraction ($<10^{-3}$) of the mass of the DS, it can power the star (see also section 5). The reason is that WIMP annihilation is a very efficient power source: 2/3 of the restmass energy of the WIMPs is converted into useful energy for the star, whereas less than 1% of baryonic restmass energy is useful to a star via fusion.

3. Building up the mass

Once a dark star is born, with an initial mass $\sim 1 M_\odot$, it accretes mass from the surrounding medium and grows as long as the dark matter fuel persists. We have studied the growth of the DS by finding its equilibrium stellar structure at every step, as we build up the DS mass all the way from its initial value to a final supermassive scale $\sim 10^7 M_\odot$. As the initial conditions for our simulations, we take a DS in which the baryons are fully ionized. We have run models for a variety of accretion rates of baryons onto the star including constant accretion rates of $\dot{M} = 10^{-1}, 10^{-2}, 10^{-3} M_\odot$/yr, as well as variable accretion rates. In this review, we will focus for specificity on the case where dark stars are accreting matter at a (constant) rate of $\dot{M} = 10^{-3} M_\odot$ yr^{-1} in a host minihalo of $10^6 M_\odot$, forming at a redshift of $z = 20$, and denoted as 'SMH',

$$\text{SMH (Minihalo)} : \dot{M} = 10^{-3} M_\odot \text{ yr}^{-1}, \quad \text{host halo of } 10^6 M_\odot. \tag{8}$$

Although not discussed in this review, we also studied a second case, labeled 'LMH,' in which we considered DSs which are accreting at a higher rate of $\dot{M} = 10^{-1} M_\odot$ yr^{-1} in a larger host halo of $10^8 M_\odot$ with a formation redshift of $z = 15$,

$$\text{LMH (Large Halo)} : \quad \dot{M} = 10^{-1} M_\odot \text{ yr}^{-1}, \quad \text{host halo of } 10^8 M_\odot. \tag{9}$$

The results for this case can be found in our series of papers for both the polytropic approximation [13–15] and using the MESA stellar evolution code [16].

4. Equilibrium structure of the dark star

Dark stars are in hydrostatic and thermal equilibrium. In our work, we adjust the DS radius such that the DM heating matches the radiated luminosity of the DS. In this section, we describe the basic equations and their implementation using both of our approaches—our earlier polytropic models and our later 1D stellar structure (MESA) models.

[10] Simulations would be required to follow the exact onset of the dark star phase in hydrostatic equilibrium. This is an important project for the future.

4.1. Basic equations

In a numerical code for stellar structure, one key requirement is the hydrostatic equilibrium of the star. This is imposed at each time-step during the accretion process,

$$\frac{\mathrm{d}P}{\mathrm{d}r} = -\rho(r)\frac{GM(r)}{r^2}, \tag{10}$$

where P denotes the pressure, $\rho(r)$ is the total density and $M(r)$ is the mass enclosed in a spherical shell of radius r.

Polytropic approach: as mentioned in the introduction, in our initial studies, we assumed that the star can be described as a polytrope as in equation (2), $P = K\rho^{1+1/n}$. We found that the energy transport is initially convective with polytropic index $n = 3/2$, but as the star approaches the zero age main sequence (ZAMS) it becomes radiative with $n = 3$. The code interpolates between $n = 3/2$ and $n = 3$ to account for the shift in energy transport as the star grows in mass. This transition happens around (100–400)$M_\odot$, after which DSs are radiative, following ($n = 3$)-polytropes. We can determine the temperature at each point in the radial grid via the equation of state of a gas-radiation mixture,

$$P(r) = \frac{k_\mathrm{B}\rho(r)T(r)}{m_u\mu} + \frac{1}{3}aT(r)^4 \equiv P_g + P_\mathrm{rad}. \tag{11}$$

Here k_B is the Boltzmann constant, m_u is the atomic mass unit and $\mu = (2X + 3/4Y)^{-1}$ is the mean atomic weight. In all resulting models $T \gtrsim 10^4$ K except near the surface, so we use the mean atomic weight for fully ionized H and He. We assume a H mass fraction of $X = 0.76$ and a He mass fraction $Y = 0.24$.

At each point in the radial grid, $T(r)$ and $\rho(r)$ are used to determine the Rosseland mean opacity κ from a zero metallicity table from OPAL [73], supplemented at low temperatures by opacities from [74] for $T < 6000$ K. The location of the photosphere is determined by the hydrostatic condition

$$\kappa P = \frac{2}{3}g, \tag{12}$$

where g is the surface gravity. This corresponds to a point with inward integrated optical depth $\tau \sim 2/3$; here the local temperature is set to T_eff and the stellar radiated luminosity is therefore

$$L_* = 4\pi R_*^2 \sigma_\mathrm{B} T_\mathrm{eff}^4, \tag{13}$$

with R_* being the photospheric radius. The thermal equilibrium condition is

$$L_* = L_\mathrm{tot} \tag{14}$$

where L_tot is the total luminosity output from all energy sources as described below in section 4.2.

Starting with a mass M and an estimate for the outer radius R_*, the code integrates equations (10) and (11) outward from the center. The initial conditions for the central temperature and gas density were taken from the protostellar gas profile

of [10]. The total luminosity output $L_{\rm tot}$ is compared to the stellar radiated luminosity, as in equation (13) and the radius is adjusted until the condition of thermal equilibrium is met (a convergence of 1 in 10^4 is reached). To re-iterate, we find that, initially, the DSs are in convective equilibrium; from (100–400)$M_\odot$ there is a transition to the radiative ($n = 3$)-polytrope case.

Stellar evolution using MESA: in the MESA stellar code[11], the equilibrium equations are built in, as are opacities and tabulated equations-of-state, see [75, 76]. In MESA, an initial model is specified by the (stellar) mass, a uniform composition, a luminosity, and a central temperature $T_{\rm c}$ low enough to prevent nuclear burning. Then, the total mass depends only on the central density, ρ_c. The initial guess for ρ_c assumes an $n = 3/2$ polytrope, as for a fully convective star, although this assumption is relaxed in the subsequent search for a pre-main-sequence model, by using MESA's routines for solving the equations of stellar structure, equation of state, and MLT (mixing-length theory) for the treatment of convection, in order to find the ρ_c for the corresponding mass. In MESA, the star grows by accreting material at a user-specified rate, according to our choice in equations (8) and (9). The accreted material is set to have the same entropy than the surface layers of the model, so the accretion does not directly heat the surface, i.e. we adopt photospheric boundary conditions. In order to study the effect of DM heating, we have used MESA's `other_energy_implicit` interface to include the energy deposited in the model due to DM annihilation. This 'extra energy' (which, in fact, is the only energy source for our MESA dark star models) is added self-consistently during each time step, in the same way that energy due to nuclear reactions would be. We note that, for our MESA models, we assume that DM is replenished due to a continuous infall of DM on centrophilic orbits within the minihalo. Those centrophilic orbits pass arbitrarily close through the halo center (see also section 4.3.2). Thus, we adopt the same assumption as in [15], that paper on which we have based our comparison between MESA's results and polytropes. Detailed results of our calculations and comparison to the polytropic models are published in [16], a summary of which is presented in section 5. Work is in progress to include into MESA the effects of DM capture via nuclei in the dark star, as well as nuclear fusion. The results of this analysis will be presented in a future publication.

4.2. Energy sources

There are four possible contributions to the DS luminosity:

$$L_{\rm tot} = L_{\rm DM} + L_{\rm grav} + L_{\rm nuc} + L_{\rm cap} \tag{15}$$

from annihilation of adiabatically contracted DM, gravitational contraction, nuclear fusion, and annihilation by captured DM, respectively. The first source, heating due to DM annihilation in the course of adiabatic contraction, dominates from the time of DS formation until the DM runs out,

$$L_{\rm DM} = \frac{2}{3}\frac{1}{m_\chi}\int \rho(r)^2_{\rm DM}\langle\sigma v\rangle dV \tag{16}$$

where m_χ is the mass of the DM particle, $\rho_{\rm DM}$ is the ambient dark matter density inside of the star calculated via adiabatic contraction (which will be depleted unless the loss cone is refilled, see section 4.3.2.). Here $\langle\sigma v\rangle$ is the annihilation cross section with units of cm^3 s^{-1}. Adiabatic contraction is discussed in section 4.3.2 and the initial DM density profile is discussed in section 4.3.1.

Once the DM fuel runs out, the star contracts in order to maintain pressure support, and the DS phase is over. The contribution $L_{\rm grav}$ due to gravitational energy release briefly powers the star. Then, as the star contracts, the density and temperature increase to the point where nuclear fusion begins. For the polytropic calculation, we included deuterium burning starting at 10^6 K, hydrogen burning via the equilibrium proton–proton cycle [77], and helium burning via the triple-alpha reaction [78].

Only as the star starts to collapse (en route towards the fusion-powered main sequence), do the stellar densities become large enough to efficiently capture DM. The captured DM then slows down the collapse and for some time can power the star. WIMPs from far out in the halo have orbits passing through the star. The DM can then scatter off hydrogen and helium and lose enough energy to become bound to the star. In short order the DM thermalizes with the star (see section 2). The captured DM forms a Boltzmann distribution $\rho_{\rm cap}$ inside of the star. The captured DM's annihilation rate will equal the capture rate with

$$L_{\rm cap} = 2m_\chi\Gamma_{\rm cap} = 2f_Q\int {\rm d}V\,\rho^2_{\rm cap}\langle\sigma v\rangle/m_\chi \tag{17}$$

and again $f_Q = 2/3$. The factor of 2 reflects the fact that the energy per annihilation is twice the WIMP mass. Owing to the stars' more compact shape, DSs powered by captured DM are much hotter and denser than those powered by gravitationally captured DM.

4.3. Dark matter densities

We turn now to the question of the dark matter density inside DSs, from their first formation in the centers of DM minihaloes, and then forward in time as they grow in mass.

4.3.1. Initial profile. The first stars form inside $\sim 10^6 M_\odot$ halos. As mentioned above, there is still some uncertainty about the exact inner slope of a DM halo [79–81]. In our studies, we have used a Navarro, Frenk, & White (NFW) profile [62] for concreteness,

$$\rho(r) = \frac{\rho_0}{r/r_s(1 + r/r_s)^2}, \tag{18}$$

where ρ_0 is the 'central' density and r_s is the scale radius. The density scale, ρ_0 can be re-expressed in terms of the critical density of the Universe at a given redshift, $\rho_c(z)$ via

$$\rho_0 = \rho_c(z)\frac{200}{3}\frac{c^3}{\ln(1 + {\rm c}) - {\rm c}/({\rm c} + 1)}, \tag{19}$$

[11] MESA is open source software and can be downloaded from http://mesa.sourceforge.net

where $c \equiv r_{\rm vir}/r_s$ is the concentration parameter and $r_{\rm vir}$ is the virial radius of the halo. We considered a variety of values for the concentration parameter for the polytropic case and found little dependence. For the MESA calculation, we chose a canonical value of $c = 3.5$.

It is important to reiterate that the results of our work on DSs do **not** depend on the shape of the initial density profile. Indeed, some of us showed in [60] that a DS results, regardless of the details of the initial density profile, even for the extreme and unrealistic case of a cored Burkert profile.

4.3.2. Adiabatic contraction. As the baryons start to collapse into a protostellar cloud at the center of the DM halo, the DM responds to the changing gravitational potential well. We use adiabatic contraction (AC) to describe this increase in DM density. The baryons radiate energy and lose angular momentum. In contrast, the DM particles conserve certain adiabatic invariants.

We outline here the Blumenthal method (see [82–84]). We consider the case of circular orbits (noting that it also applies to purely radial orbits) and assume that orbits do not cross. A DM particle orbiting further out will not cross the orbit of a DM particle further in which implies that $m(r_i)_\chi = m(r_f)_\chi$ where $m_\chi(r)$ is the mass of DM interior to a radius r. Here r_i is the initial radius before the baryons fall in and r_f is the radius of the DM particle after infall. With the conservation of angular momentum and energy, $r\,m(r)$ is constant for each DM particle, where r is the radius of the orbit. The mass consists both of a dark matter component m_χ and a baryonic component $m_{\rm B}$ with $m = m_\chi + m_{\rm B}$. As the baryons fall in, r must then decrease. For instance, if the mass of the Sun grew slowly, the Earth's orbit would shrink.

The Blumenthal method, despite its simplicity, is remarkably accurate in estimating the effect of adiabatic contraction in general. Given an initial distribution of dark matter and baryonic matter, we can then find the final DM profile if we also know the final baryonic distribution, which we obtain from the gas profile calculated in the first-star-simulation of [10]. By performing exact calculations for spherical halos [60], we found that the simple Blumenthal method [82–84] gives reliable results for the final DM densities up to a factor of two; others have confirmed this conclusion [22, 28, 59].

In our early work, we probably underestimated the lifetime of the DM inside the star due to AC. At first we treated the DM halo as spherical and ran up the DS mass to the point where the DM initially inside the star was entirely consumed by annihilation. The DS mass at this point is $O(10^3)M_\odot$ after a lifetime of ∼300 000 years, and the amount of DM consumed has only amounted to $\sim 1 M_\odot$. In a spherical DM halo, the orbits of DM particles are planar rosettes [85], conserving energy as well as all three components of angular momentum; consequently the central hole (or 'empty loss cone') that results from DM annihilation cannot be repopulated once it is depleted. However, it is well known that DM halos formed in hierarchical structure formation simulations are not spherical but are prolate-triaxial [86–90] with typical axis ratios of (short-axis)/(long-axis) ∼ 0.6–0.8. In triaxial potentials, the orbits do not conserve any component of angular momentum. In particular, there are two families of 'centrophilic orbits' (box orbits and chaotic orbits) which oscillate back and forth through the potential and can travel arbitrarily close to the center [91–97]. These orbits have the low angular momentum necessary for replenishing DM in the center, implying that the duration of a DS phase could increase by many orders of magnitude, from ∼300 000 years (see section 5 and figure 2) to a timescale many orders of magnitude longer, depending on the cosmological evolution of the minihalo hosting the DS.

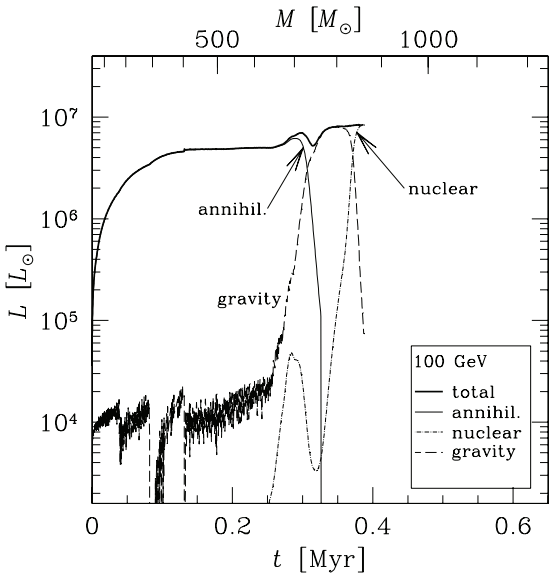

Figure 2. Luminosity evolution of dark stars for the case of a 100 GeV WIMP mass as a function of time (*lower scale*) and stellar mass (*upper scale*). Results were obtained assuming polytropic interiors for the DS. The solid top curve is the total luminosity. The lower curves give the partial contributions of different sources of energy powering the star without capture. The total luminosity is initially dominated by DM annihilation (the total and annihilation curves are indistinguishable until about 0.3 Myr after the beginning of the simulation); then gravity dominates, followed by nuclear fusion. In this plot, we have cut off the DM heating by hand at 0.3 Myr when the DS mass approaches 850 $M_\odot$, as one example of a final possible DS. In reality, the DM annihilation continues as long as the DM reservoir is replenished (depending on the DM environment of the particular star); thus the DS could continue to grow for a longer time and the final DS mass could be many orders of magnitude larger than in the plot shown here. The purpose of this figure is to show the full evolution of an illustrative example of a dark star and its many contributing heat sources. (Figure reproduced with permission from [14]).

Several studies of the shapes of DM halos have shown that when baryons condense into the center of the DM halo, the shape of the inner region ($0.3 \times r_{\rm vir}$) becomes nearly spherical [98–100]. This raises the concern that the formation of the DS itself would lead the DM halo to convert from being triaxial back to being spherical before the DS reaches supermassive size. In a series of papers, [101, 102] carried out a detailed statistical analysis of the orbital properties of DM particles in triaxial and prolate-triaxial halos in which baryonic components were grown adiabatically. They analyzed over 20 000 randomly selected halo orbits as a function of radius using an automatic orbit classification tool that relies

on the fundamental oscillation frequencies of each orbit (using frequency mapping), see [103, 104]. It has been shown in [101, 102] that the orbits of DM particles remain primarily centrophilic ('box' orbits and chaotic orbits) in the inner-most regions of the DM halo despite the fact that the halos become quite close to (but not exactly) spherical. More precisely, it has been shown in [101] that over 50% of the orbits overally are centrophilic which, after a few orbital periods, will get arbitrarily close to the center of the potential. More recently, [105] analyzed DM halo particles in a fully cosmological hydrodynamical simulation of a disk galaxy, part of the McMaster Unbiased Galaxy Simulations [106]. They found that, in the fully cosmological simulations, DM halos became even more spherical than when the baryonic components were grown adiabatically, nonetheless an even more significant fraction of DM halo particles remained on box and chaotic orbits, indicating that, even when the full hierarchical merger history of a halo is considered, DM particles will continue to be on orbits that penetrate to the central cusp, thereby continuing to provide heat for the DS.

As a consequence of the prolonged period of dark matter heating, supermassive DSs (SMDSs) can result, with masses up to 10^5–$10^7\,M_\odot$ and luminosities up to 10^8–$10^{11}\,L_\odot$. The amount of dark matter required inside the star to sustain long enough DM heating to reach these stellar masses is still small; e.g. $\sim$100 $M_\odot$ for a $10^5\,M_\odot$ SMDS for an accretion rate of $\dot{M} = 10^{-1}\,M_\odot$/yr and $\sim 10^4\,M_\odot$ for an accretion rate of $\dot{M} = 10^{-3}\,M_\odot$/yr, out of a total $10^6\,M_\odot$ halo.

In reality, DSs will form in a variety of environments and experience mergers during their life times. Such mergers could disrupt or enhance the growth of SMDSs at various stages, resulting in DSs of a variety of masses.

4.3.3. Dark matter capture. In the previous section, we have only discussed the dark matter brought into the DS purely by gravity via adiabatic contraction. However, the DM reservoir inside the DS can be refueled by DM capture, in addition. This refueling requires an additional piece of particle physics: scattering of DM off the nuclei inside the star. This is the same elastic scattering that is the origin of searches for detectable signals in dark matter 'direct detection experiments', such as DAMA, Xenon-based detectors, SUPERCDMS, CRESST, PICO, and many others. The role of captured DM in DSs was first noticed simultaneously in [21, 61]. The capture rate is sensitive to two uncertain quantities: the scattering cross section of WIMP interactions with the nuclei and the background DM density.

The cross section for elastic scattering depends on the coupling of DM to ordinary matter. The two cases most often considered are 'spin-independent' (SI) and 'spin-dependent' (SD) scattering. For WIMP masses above $\sim$1 GeV, the constraints on spin-independent scattering are much stronger than for spin-dependent scattering. Hence, we consider here the optimal case for capture in DSs, namely SD scattering. The PICO experiment [107] has preliminary constraints which are the most restrictive for SD scattering,

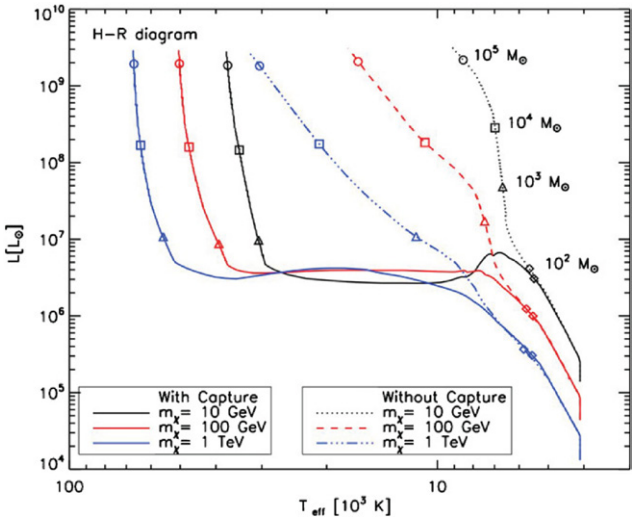

Figure 3. Hertzsprung–Russell diagram for DSs forming in SMH, as defined in equation (8), and a variety of WIMP masses as labeled for the two cases: (i) 'without capture' but with extended adiabatic contraction (dotted lines), assuming no significant depletion of DM due to annihilation, which is equivalent to assuming a replenishment of DM due to centrophilic orbits, as explained in text; (ii) 'with capture' (solid lines). Results were obtained assuming polytropic interiors for the DS. The case with capture is for product of scattering cross section times ambient WIMP density $\sigma_c \bar{\rho}_\chi = 10^{-39}\,\mathrm{cm}^2 \times 10^{13}\,\mathrm{GeV\,cm}^{-3}$ (the maximum allowed cross section for all WIMP masses and the maximum reasonable ambient density for 100 GeV WIMPs). Given these values, DSs must become dense enough for DM capture to happen. This explains the horizontal lines in the evolution of the case 'with capture'. Labeled are also stellar masses reached by the DS on its way to becoming supermassive. The final DS mass was taken to be $1.5 \times 10^5\,M_\odot$ (the baryonic mass inside the initial halo), but could vary from halo to halo, depending on the specifics of the halo mergers (figure reproduced with permission from [15]).

$\sigma < 10^{-39}\,\mathrm{cm}^2$ for $m_\chi = 30$ GeV (and much weaker for other masses). For $m_\chi \sim 1$ GeV, the bound is roughly $\sigma < 10^{-37}$ cm^2, see [107–109][12].

In the interesting case of a high DM density environment, the additional DM power due to captured DM can allow the DS to keep growing, to the point where SMDSs of mass $>10^5\,M_\odot$ can result, see [15]. Thus, SMDSs can arise due to two separate DM populations: the DM brought in via gravity (extended AC) or the DM brought in via capture. The two different types of SMDSs are quite different objects, as we show below.

[12] Spin-independent scattering has much stronger constraints. For $m_\chi \sim 1$ GeV, CDMSlite [110] constrains the cross section to be less than roughly 10^{-40} cm^2. For $m_\chi = 30$ GeV, LUX constrains the cross section to be less than 4×10^{-46} cm^2 [111]. Colliders (assuming effective operators with a large cut off) can also in some cases provide constraints; though the validity of the effective operator approach is not general [112, 113]. In those cases where the effective operator approach is valid, CMS and ATLAS constrain the spin-dependent cross sections to $\sigma < 10^{-40}$ cm^2 for $m_\chi < 100$ GeV and this weakens to $\sigma < 10^{-39}$ cm^2 for m_χ above a few hundred GeV. Also, for energies (DM masses, respectively) above the cut off mass—given by the ratio of mediator mass to coupling constant—, the constraints should not be trusted, since an effective operator approach is invalid.

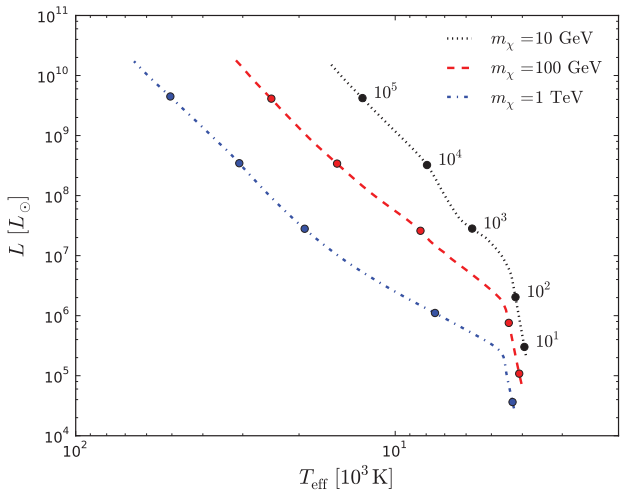

Figure 4. Hertzsprung–Russell diagram for DSs forming in SMH (defined in equation (8)) and a variety of WIMP masses, using the MESA stellar evolution code. The calculations assume extended adiabatic contraction and no significant depletion of DM due to annihilation. DM capture is not considered. Labeled are stellar masses reached by the DS on its way to becoming supermassive; see also [16].

5. Results of stellar structure analysis

In this section, we discuss the results of our stellar structure analysis for a variety of cases. We show results for both the case of 'extended AC' (where DM is brought into the star via gravity only), as well as the case 'with capture' (where DM is captured in the star via elastic scattering). We consider a range of WIMP masses $m_\chi = 10$ GeV, 100 GeV, and 1 TeV. We show results using our two approaches: polytropic stellar models and models obtained with the MESA stellar evolution code. In this section, we use the accretion rate and halo size defined in equation (8); for other cases our results can be found in our series of papers. Figures 2–5 show the stellar models that are the result of our analysis. Figures 2 and 3 were obtained using polytropic stellar interiors [15], while figures 4 and 5 are our results using the MESA stellar evolution code [16].

Figure 2 shows the luminosity evolution of a DS for the case of adiabatically contracted DM only (no capture) for polytropic interiors and assuming that the DM runs out when the star reaches about 800 $M_\odot$ at roughly 0.3 Myr after the beginning of the simulation. This cutoff in the lifetime of the DS phase was obtained using the overly conservative assumption that DM would run out inside the DS at that time (based on the incorrect assumption that the DM halo is spherical; see the discussion in section 4.3.2). In reality, the DS could keep growing for a much longer time, depending on its DM environment. The various contributions to the luminosity in equation (15) are plotted as well as the total luminosity (solid curve). The total luminosity is initially dominated by DM annihilation; then gravitational contraction dominates, followed by nuclear fusion.

The Hertzsprung–Russell diagram resulting from our studies using polytropic interiors in [15] is shown in figure 3. The DS travels up to increasingly higher luminosities as it becomes more massive due to accretion. As the mass increases, so does the surface temperature. In the cases 'with capture', we have taken the (overly conservative) assumption that the DM from adiabatic contraction is depleted after ∼300 000 yrs as in our earlier papers; then the luminosity plateaus for some time, while the DS contracts until, eventually, it is dense enough to capture further DM.

We note that, for the case 'without capture', the tracks in the H–R diagram are unchanged by varying the accretion rate: only the time it takes to get from one mass stage to the next changes, but the curves we have plotted apply equally to all accretion rates. The Hertzsprung–Russell diagram obtained with MESA can be found in figure 4 for the case of extended AC. DM capture and fusion have not yet been included, and work is in progress to implement these as well. In general, we found remarkably good overall agreement with the basic results of the polytropic models; however there are some differences. Using MESA, we found that, in the mass range of 10^4–$10^5\,M_\odot$, our DSs are hotter by a factor of 1.5 than those in [15], are smaller in radius by a factor of 0.6, denser by a factor of 3–4, and more luminous by a factor of 2. Thus, the overall colors of our DSs are not very different from the polytropic models, while the higher luminosities we find improve the prospect of observability of DSs with upcoming space telescopes, such as the JWST.

In the HR diagrams of figure 3 and 4, the curves with higher values of WIMP mass m_χ lie to the left of the curves with lower m_χ. This can be understood as follows. The DM heating rate in equation (1) scales as $Q \propto \rho_\chi^2/m_\chi$. Hence, to reach the same amount of heating and achieve the same luminosity at higher m_χ, the DS must be at higher WIMP density, i.e. the stellar radius must be smaller, the DS is hotter, and the corresponding surface temperature $T_{\rm eff}$ is higher. Also, for higher m_χ the amount of DM in the star is smaller since the star is more compact for the same number of baryons, but $\rho_\chi \propto n^{0.81}$, see equation (5).

The density and pressure distribution within a supermassive DS of $10^5\,M_\odot$ obtained using the MESA code can be found in figure 5. As expected from earlier results, the DM density is roughly three orders of magnitude below the baryonic gas density, i.e. the DM mass contribution in DSs is very small, see left-hand-plot. For the example shown in figure 5, the total mass in DM only amounts to about $20M_\odot$, or 0.02% of the DS mass. The shape of both density profiles as well as their absolute magnitude agrees excellently with the results in figure 3, case 1 of [14]. The right-hand-plot of figure 5 shows the total pressure inside the DS as a function of radius. To this end, we plot MESA's accurate result together with the known run of polytropes of index $n = 3/2$, $n = 3$ and $n = 4$, respectively. Except close to the surface, we can see that supermassive DSs can be very well approximated by ($n = 3$)-polytropes, as has been found in the earlier work of [14, 15], and as we have described above. In fact, our MESA results confirm even the overall evolution of the internal pressure distribution and energy transfer of DSs on their way of becoming supermassive, as follows. While MESA does not

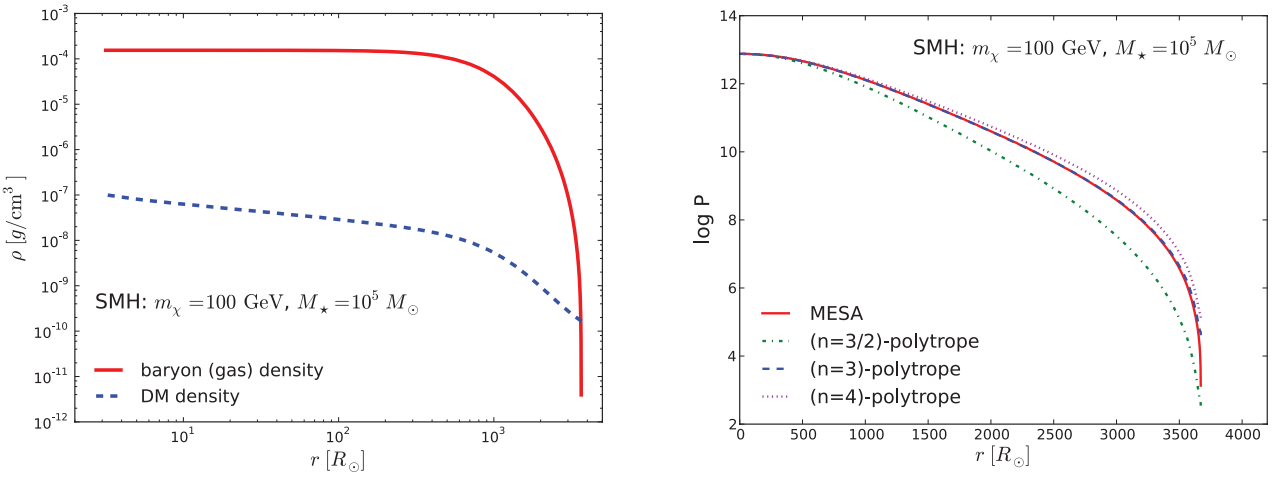

Figure 5. A dark star with mass $10^5\,M_\odot$ forming in SMH and WIMP mass 100 GeV: results were obtained using the MESA stellar evolution code. *Left-hand plot:* Baryonic gas and DM density profiles within the DS. The DM density is roughly three orders of magnitude below the gas density. *Right-hand plot:* Stellar total pressure as a function of stellar radius: comparison of MESA's results with polytropes of index $n = 3/2$, $n = 3$ and $n = 4$, assuming the same central pressure and density. The figure shows that supermassive DSs can be very well approximated by ($n = 3$)-polytropes, confirming earlier results. Note the different x-axis scale in the two figures; see also [16].

need to rely on the assumption of polytropic equations-of-state, we can still define an 'effective polytropic index' via

$$n_{\rm eff} = \left[\frac{\log(P/P_c)}{\log(\rho/\rho_c)} - 1\right]^{-1}, \qquad (20)$$

where P and ρ are the exact MESA values for the pressure and density, with P_c and ρ_c their values at the DS center. For low-mass DSs with a stellar mass around (10–20)$M_\odot$, $n_{\rm eff}$ is close to the value of 3/2, appropriate for a fully convective star. This value steadily increases to above $n_{\rm eff} = 2$ for more than $100M_\odot$. Around this point, the luminosity due to radiation transfer starts to be of the order of the luminosity due to convection, i.e. $L_{\rm rad} \sim L_c$. As the DS continues its mass growth, $n_{\rm eff}$ continues to approach a value of 3, and $L_{\rm rad}$ becomes increasingly important. The energy transport in supermassive DSs is thus dominated by radiation transfer.

In a beautiful paper in 1963, Hoyle and Fowler [114] studied supermassive stars in excess of $10^3\,M_\odot$ and found results germane to our work. They treated these as ($n = 3$)-polytropes, dominated by radiation pressure, and found the following results: $R_* \sim 10^{11}(M_*/M_\odot)^{1/2}(T_{\rm c}/10^8\ {\rm K})^{-1}$ cm, $L_*/L_\odot \sim 10^4\ M_*/M_\odot$, and $T_{\rm eff} \sim 10^5(T_{\rm c}/10^8{\rm K})^{1/2}$ K. While some of the details of their calculations differ from ours, taking the central temperature appropriate to DSs in the above relations roughly reproduces our results (to $O(1)$). By using the temperature appropriate to DSs with extended AC ($T_{\rm c} \sim 10^6$ K) rather than the much higher central temperature ($T_{\rm c} > 10^8$ K) appropriate to nuclear power generation, the above relations show that DSs have much larger radii and smaller surface temperatures than fusion-powered stars. The fact that DSs are so fluffy objects makes them resilient against general-relativistic instabilities, since general-relativistic corrections, which would act in the direction of destabilizing supermassive stars, scale as GM_*/R_*. The upper limit on the allowed stellar mass is thus larger for DSs.

For the cases with capture, we take $\sigma_c\bar{\rho}_\chi = 10^{-39}\ {\rm cm}^2 \times 10^{13}$ GeV cm^{-3} (the product of the maximum allowed scattering cross section from direct detection experiments, and the maximum reasonable ambient density for 100 GeV WIMPs). With these parameters, DSs must become dense enough for DM capture to happen. The cases with capture all take place at higher stellar densities than the cases without; the density must be high enough to be able to capture WIMPs. Consequently, the surface temperature is larger and accretion is shut off more easily by radiation coming from the star. Between 50 000 K and 100 000 K feedback effects were included in the polytropic case, and they act to reduce the accretion rate, but they never shut it off entirely for densities above 5×10^{10} GeV cm^{-3}. In reality, a star that is moving around can sometimes hit pockets of high $\bar{\rho}_\chi$ (where it is DM powered and grows in mass) and sometimes hit pockets of low $\bar{\rho}_\chi$ (where fusion takes over). As long as the ambient density remains at least this large, the star can reach arbitrarily large masses and eat the entire baryonic content of the halo.

The capture mechanism depends on the product of scattering cross section times ambient density, $\sigma_c\bar{\rho}_\chi$, rather than on either of these quantities separately. Hence, our current discussion could trade off ambient density versus cross section. For example, the product is the same for $\bar{\rho}_\chi = 5 \times 10^{10}$ GeV cm^{-3} and $\sigma_c = 10^{-39}$ cm^2 as it is for $\bar{\rho}_\chi = 10^{13}$ GeV cm^{-3} and $\sigma_c = 5 \times 10^{-42}$ cm^2.

Above $\sim 100M_\odot$, one can see that the stellar luminosity scales as $L_* \propto M_*$ and is the same for all models for a given stellar mass; this statement is essentially true for all stars no matter the power source. The reason is that at these masses, the star is essentially radiation pressure supported throughout. This same scaling in supermassive stars was already noticed in [114]. We confirmed with MESA that the luminosity of DSs stays comfortably below the Eddington limit luminosity (which scales as $L_{\rm Edd} \propto M_*$) for most of the DS evolution and tracks it just below at the supermassive end.

This and other details of the stellar structure of the first DSs will be presented in [115].

The caveat in the above discussion is that in order to continue to grow, the DM orbits must continue to penetrate into the middle of the DS for a greater length of time; it is the DM heat source that keeps the DS cool enough to allow it to continue to accrete baryons. Additionally, the assumption that baryons continue to accrete onto the DS must continue to hold. Yet, in the time frame required, the original $10^6 M_\odot$ minihalo will merge with its neighbors, so that both the baryon and DM densities are disturbed. These mergers could affect the DS in one of two ways: either they provide more baryons and DM to feed the SMDS so that it ends up being even larger, or they disrupt the pleasant high DM environment of the SMDS so that it loses its fuel and converts to an entirely fusion-powered star. Continued growth of the DS is quite plausible since simulations with massive black holes in mergers show that they prefer to sit close to the center of the density distribution, or find the center in a short time after the merger.

Someday detailed cosmological simulations will be required to answer this question. Individual DSs in different halos may end up with a variety of different masses, depending on the details of the evolution of the halos they live in. The case studied in [15] and [16] is clearly a simplistic version of the more complicated reality, but illustrates the basic idea that supermassive stars may be created by accretion onto DSs, either with or without capture.

5.1. Response to criticism

Before we move on to describe the observable properties of dark stars, we would like to address some recent critiques of the feasability of a DS phase. The concern is whether DSs are ever able to form at all; we feel that the issues raised in the criticism are easy to address. We refer to a note on the arXiv for a more quantitative response, see [116].

First, [27] and [117] have performed simulations of collapsing protostellar clouds and noted that the collapse continues past the hydrogen density quoted in [12] as the point where DM heating starts to dominate. This fact led to the incorrect conclusion that DM annihilation is not potent enough for the establishment of a DS in hydrostatic equilibrium, powered by DM heating. However, there is in reality no disagreement between the results of these simulations and the existence of a dark star. Once the DM power dominates, the protostellar object must indeed collapse further before it becomes a real star, in hydrostatic and thermal equilibrium. Specifically, the objections have arisen because for 100 GeV WIMPs, the simulations of [27] and [117] found that the collapse continues past a hydrogen density $n_h = 5 \times 10^{14}\,\mathrm{cm}^{-3}$, which is the limit of their simulations. Indeed, we agree in [13] and [14] that the cloud continues to collapse past this point; and we find that the initial dark star forms later, when the hydrogen density is $n_h \sim 10^{17}\,\mathrm{cm}^{-3}$, three orders of magnitude higher than the limits of the simulations. The aforementioned simulations are unable to reach densities this high, and are therefore unable to directly address the dark star regime. A very interesting project would be to push the simulations further to observe the actual formation of the dark star.

Second, concern has been addressed in [118] that the DM accessible to the DS at the centers of minihalos may run out rapidly enough, so as to limit the DS phase to only a few thousand years. However, as we have described in section 4.3.2, typically half of the dark matter orbits come in from far outside the small region near the halo center that is studied in these simulations; these dark matter particles do indeed continue to replenish the DM required for DSs to grow.

Third, a growing body of literature finds that the accretion disk around the first protostars can fragment, leading to the possible formation of multiple systems and removal of the central object from the DM cusp, see e.g. [119–121]. However, the inclusion of DM heating in [117] resulted in a stabilizing effect, preventing fragmentation around the central protostar. Future studies with high enough resolution to capture the mutual dynamical effects of baryons and DM in these central regions will be needed.

Finally, in existing simulations in the papers criticizing our work, there are inaccuracies in the energy injection that should be corrected: the prescriptions for the treatment of the effect of DM annihilation energy injection into the primordial protostellar gas are valid for particle energies in the keV range, which are lower than those expected from WIMP decay. We note that in our original work in [12], we required that the WIMP annihilation products have at least 80 radiation lengths in the DS—this is overkill in ensuring that they will be trapped and heat the protostar. Our work did take into account the electromagnetic cascades experienced by WIMP annihilation products with energies exceeding 100 s of MeVs. It is the electrons with energies above around 280 MeV and photons above around 100 MeV which initiate a further electromagnetic cascade in their hydrogen environment. Lower-energetic electrons lose their energy pre-dominantly by ionization, while lower-energetic photons Compton-scatter off electrons. The correct treatment of energy injection within the molecular cloud in which the first star forms is thus critical. Ideally, one would numerically compute the stages of energy injection at different radii throughout the star.

6. Detectability of dark stars with the James Webb Space Telescope

In [15] and [122], some of the authors of this paper, as well as [29], studied the capability of the upcoming James Webb Space Telescope (JWST) to detect supermassive dark stars (SMDSs). As shown above, if the first stars are powered by dark matter heating in triaxial dark matter halos, some of them may grow to be very large $>10^6 M_\odot$ and very bright $>10^9 L_\odot$. These SMDSs would be visible in deep imaging with JWST and even the Hubble space telescope (HST) [30, 123].

The Hubble space telescope (HST) has carried out a series of deep imaging surveys (the Hubble ultra-deep field (HUDF), extreme deep field (XDF)) of a small patch of sky in the constellation Fornax in order to detect galaxies in

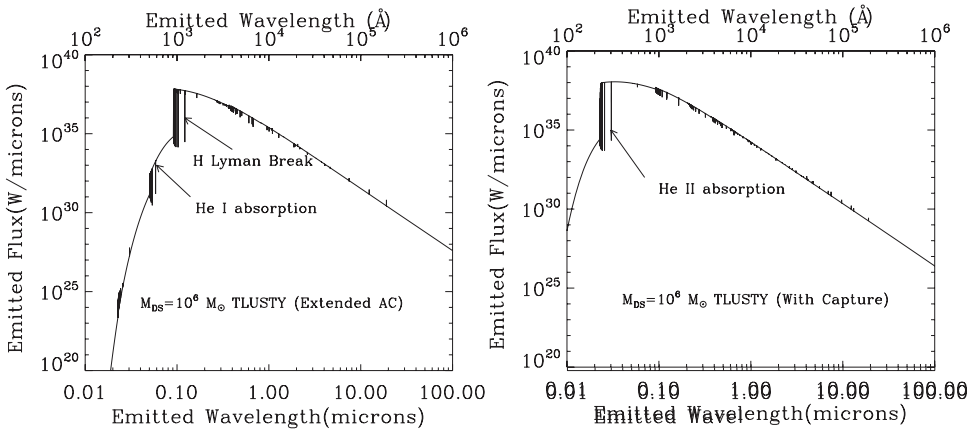

Figure 6. Expected spectral energy distribution (SEDs) of $10^6 M_\odot$ supermassive DSs. Left panel: DS with a surface temperature of 1.9×10^4 K and formed via the extended adiabatic contraction (AC) mechanism only. Right panel: with a surface temperature of 5.1×10^4 K, formed via AC and 'with capture' (figure reproduced with permission from [122]).

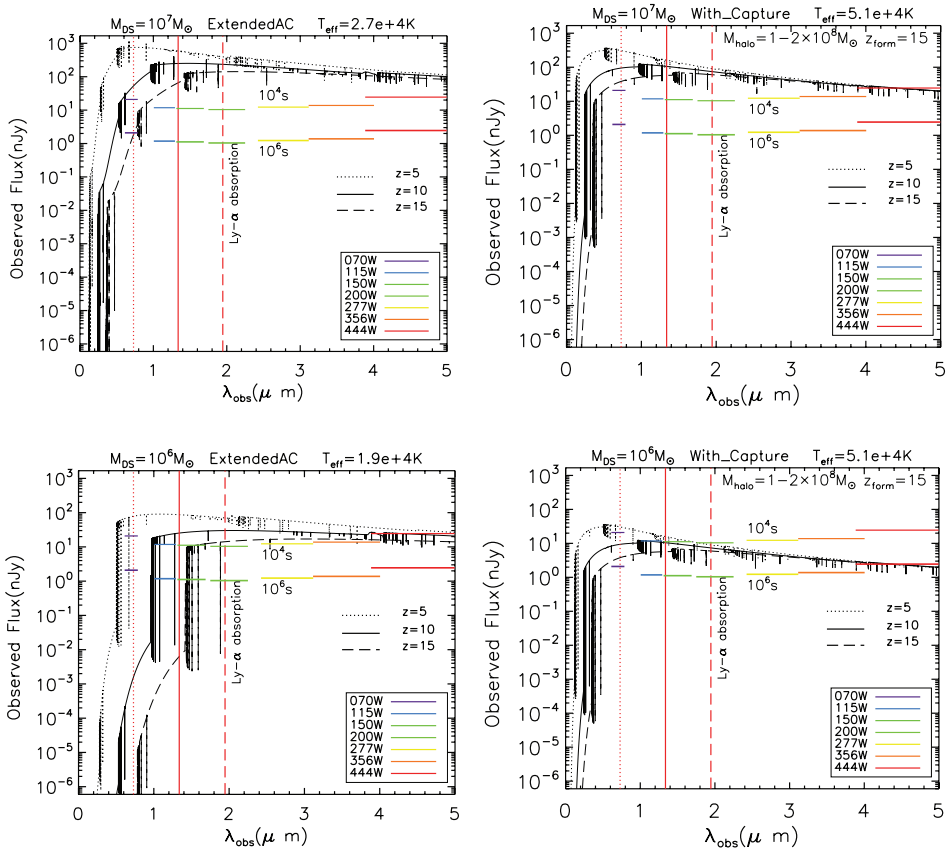

Figure 7. Spectra for supermassive DSs formed at $z_{\rm form} = 15$ (formation redshift) compared with sensitivity of JWST filters. Listed above each panel are the mass of the DS in solar masses, the formation mechanism (extended AC or 'with capture') and the surface temperature $T_{\rm eff}$. The fluxes are shown at $z = 15$ (dashed line), 10 (solid line) and 5 (dotted line) and compared to the detection limits of NirCam wide passband filters. The colored horizontal lines represent the sensitivity limits for the filters as labeled in the legend for exposure times 10^4 s (upper lines) and 10^6 s (lower lines). IGM absorption will decrease the observed fluxes for wavelengths shortward of the vertical red lines, which indicate the Lyman-α line (1216 Å) redshifted from the rest-frame of the star (figure reproduced with permission from [122]).

the early Universe using the near infrared camera WFC3 with multiple broad-band filters (centered on 1055.2 nm (Y-Band), 1248.6 nm (J-Band), and 1536.9 nm (H-band)). HST has successfully identified galaxies at redshifts $z \sim 7$ –10, using the dropout technique described below (see [124–126]).

JWST will be a large infrared telescope with a 6.5 m primary mirror and is expected to be launched in 2018. JWST is an international collaboration between NASA, the European Space Agency (ESA), and the Canadian Space Agency (CSA). Four infrared instruments are being built for JWST: the near infrared camera (NIRCam), the near infrared spectrograph

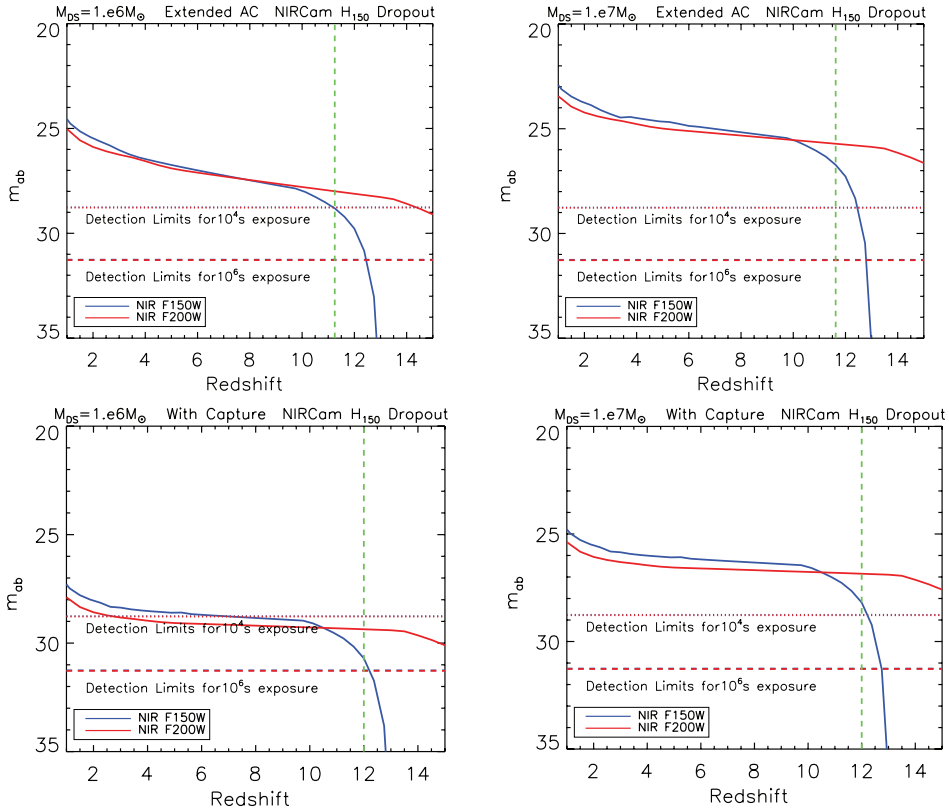

Figure 8. Supermassive dark stars with JWST as H_{150} band dropouts: Apparent magnitudes for SMDSs through the F150W (central wavelength 1505 nm) and F200W (central wavelength 2000 nm) NirCam filters. Those could be used to establish dropout detection criteria in the 12–14 redshift range. Top panel: $10^6\,M_\odot$ and $10^7\,M_\odot$ DSs formed without considering DM capture. Lower panel: $10^6\,M_\odot$ and $10^7\,M_\odot$ DSs formed including DM capture. The vertical green dashed line indicates the minimum redshift at which the DS will appear as a dropout (figure reproduced with permission from [122], where we also illustrated detectability of DSs in other wavelength bands than the ones discussed here).

(NIRSpec), the mid-infraRed instrument (MIRI), and the fine guidance sensor/ near infrared imager and slitless spectrograph (FGS-NIRISS) and are sensitive to wavelengths from 600 nm (optical red) to 28 000 nm.

In order to determine the sensitivity of the HST and JWST instruments to DSs, some of us, with the help of Pat Scott, found what SMDSs would look like [122], using the atmospheric models from [30]. The spectra of SMDSs were obtained, using the publicly available TLUSTY [127] synthetic stellar atmospheres code. This code accounts for not only the black body radiation from the photosphere of the DS, but also accounts for absorption lines arising from the cooler gas in the atmosphere of the star. The spectra for the case of a $10^6\,M_\odot$ DS that formed via the two mechanisms of extended AC and capture are shown in figure 6.

We studied the sensitivity of JWST to detect dark stars in [122]. We showed that SMDSs in the mass range 10^6–$10^7 M_\odot$ are bright enough to be detected in all the wavelength bands of the NIRCam on JWST (but not in the less sensitive MIRI camera at higher wavelengths) with ultra deep exposures of 10^6 s. Figure 7 illustrates the spectra for SMDSs and compares them to the sensitivities of JWST filters.

Also, we used sensitivity limits from previous HST surveys to place bounds on the numbers of SMDSs that may be detected in future JWST imaging surveys, following the approach of [30]. Indeed, [30] and [122] showed that SMDSs of $10^7\,M_\odot$ are so bright they would have already been detected by the HST extreme ultra deep field surveys, if they existed at redshifts of 12 or lower. The absence of a DS detection in the HST deep field surveys probably rules out supermassive DSs of this mass, but less massive DSs (e.g. $\lesssim 10^6\,M_\odot$) could exist. Also, the probability of detection depends on the unknown fraction of dark matter halos that could host a dark star.

The 'dropout' technique can be used to determine the redshift of an object that is too faint for spectroscopic study. Here the object is detected in filters centered at one (or more) frequencies but not in lower frequency filters; it is invisible in the lower frequency bands because the light has been swallowed by Lyman-α absorption. The redshift of the object can then be identified, because of the knowledge of the frequency at which the Lyman-α absorption was significant. The objects will be detectable in filters centered at higher wavelengths but not in the band including the redshift of the object due to Lyman-α absorption. Objects existing at $z \sim 10$, 12, or 14 will be detectable as J-band, H-band, or K-band dropouts, respectively

HST has been able to find objects as J-band dropouts, meaning that their redshifts are $z \sim 10$. Whereas JWST is not particularly better than HST at finding J-band dropouts, it will be significantly better at finding SMDSs as H-band and K-band dropouts at higher wavelengths, corresponding to objects at

$z \sim 12$ and 14, respectively. In the case of H-band dropouts, the object can be seen in the F200 NIRCam filter of JWST, but not in the F150 NIRCam filter. We required the difference between the broadband fluxes in the H_{150} and K_{200} filters to be greater than 1.2 AB magnitudes. We can see that the SMDSs stellar light seen with JWST's K_{200} filter is essentially unaffected by Lyman−α absorption until $z \sim 15$, whereas the IGM absorption will cut off most of the flux in the H_{150} at $z \gtrsim 11.5$ (see figure 8). Hence, SMDSs can appear as H-band dropouts.

We estimated the number of SMDSs that JWST should be able to discover. With a total survey area of 150 arcmin^2 (assuming a multi-year deep parallel survey), we found that typically the number of $10^6 M_\odot$ SMDSs expected to be discovered as H or K-band dropouts is $\sim 10^5 f$, where the fraction of early DM halos hosting a dark star is likely to be small, $f \lesssim 1$. If SMDSs survive down to $z = 10$ where HST bounds apply, then the observable number of SMDSs as H or K-band dropouts with JWST is ∼1–30.

While individual SMDSs are bright enough to be detected by JWST, standard Pop III stars (without dark matter annihilation) are not; they would instead contribute to the detectability of first galaxies with total stellar masses of 10^6–$10^8 M_\odot$. It will be interesting to re-assess DS detectability in more detail, in light of the new MESA results. Differentiating first galaxies at $z > 10$ from SMDSs may be possible with spectroscopy. As described in the next section, a new interesting method of differentiating SMDS from galaxies will take advantage of the fact that SMDSs may pulsate, with timescales of the order of months in the observer's frame. If cool, bright objects are found to pulsate, then they are likely SMDSs.

7. Dark star pulsations: a new avenue of detectability

Some of the authors of this review have embarked on the study of an entirely new avenue of DS astrophysics, namely DS oscillations and pulsations. The usage of a fully-fledged stellar evolution code like MESA permits us to study such pulsations, which are deviations from hydrostatic equilibrium, see [16]. There are traditionally two classes of stellar pulsations: acoustic modes, or p-modes, where pressure is the restoring force, and gravity modes, or g-modes, where buoyancy, i.e. gravity, is the restoring force (the limit case of 'surface gravity modes' are also called f-modes). Our analysis shows that g-modes are most likely not to be found in supermassive DSs, since their interior, albeit radiation-dominated, is subject to weak convective instability; however, p-modes are permitted. As a first step, we calculated the adiabatic pulsation periods of radial modes (i.e. those for which there is no angular dependence, so $l = 0$) with different overtone number n, where $n = 1$ is the fundamental or 'breathing' mode, and $n > 1$ are higher overtone modes. In figure 9, we plot the restframe pulsation periods as a function of DS mass for the halo environment SMH in equation (8) and a WIMP mass of 100 GeV. The periods are considerably shorter for higher overtone numbers. For the example shown in figure 9, the restframe of a DS with $10^5 M_\odot$ is at $z \simeq 14.82$. Converting to the observer's frame, the periods range from 6323 d for $n = 2$, down to 127 d for $n = 8$.

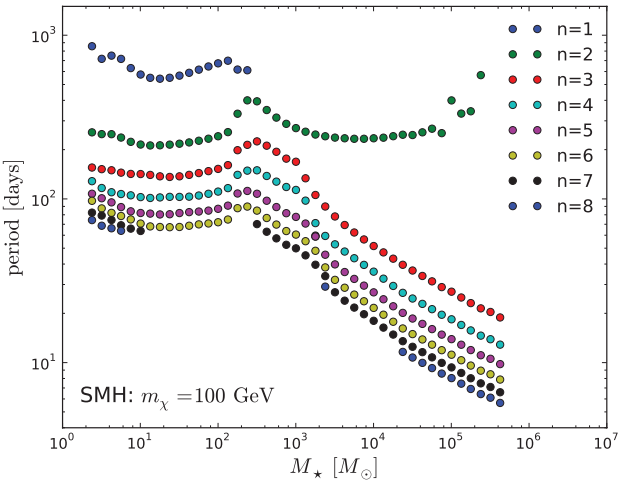

Figure 9. Radial, adiabatic pulsation periods as a function of DS mass for a WIMP mass of 100 GeV and a DS forming in SMH. The periods are given in the restframe of the DS. The curves are for different overtone number, from the fundamental radial oscillation $n = 1$ (upper-most curve) to $n = 8$ (lower-most curve); see also [16].

In general, we find that our DS models pulsate on timescales which range from less than a day to more than two years in their restframes at about $z = 15$, depending on the WIMP mass and overtone number. The pulsation periods are significantly shorter for higher WIMP mass. Converting to the observer's frame, the shortest periods we found are less than about 50 d for modes with $n > 6$ and a WIMP mass of 1 TeV [16].

Work is in progress to study DS pulsations more quantitatively, in particular possible driving mechanisms of DS pulsations. Preliminary results suggest that the traditional κ-mechanism could occur in DSs, as well. Here, pulsations are driven in layers of (partially) ionized hydrogen and helium where opacities are high. Another possible driving mechanism may be related to DM itself: small perturbations of the DSs could lead to local changes in the baryonic and DM densities, modulating the DM heating rate, in turn[13]. If SMDSs are found to pulsate, this would represent yet another way of distinguishing DSs observationally from galaxies at high redshifts. If the pulsations are detectable, DSs may in principle someday be used as novel standard candles for cosmological studies.

8. Dark stars as seeds for supermassive black holes in the Universe

Supermassive black holes (SMBHs) are ubiquitous throughout the Universe. Observations of quasars at redshifts above $z \sim 6$ suggest the presence of SMBHs in excess of $10^9 M_\odot$ at a time when the Universe was not even a billion years old [128], see also [129] for a recent discovery of a SMBH of an estimated 12 billion $M_\odot$. In addition, SMBHs are found at the centers of nearly all galaxies, and their masses appear to be well correlated with numerous properties of the spheroidal components of their host galaxies [130]. The origin of the scaling relations

[13] This would be akin to the ε-mechanism in normal stars, where fusion in the stellar cores can be subject to variation due to local temperature changes, resulting in stellar pulsations.

between host galaxies and their SMBHs remains an actively researched topic. One issue that remains unsolved is the origin and mass distribution of the seed black holes that eventually grow into supermassive ones. It is generally believed that there is not enough time for stellar mass black holes that result from the death of massive stars to accrete at a high enough rate to grow into the SMBHs that power high redshift quasars. Some physical mechanism is required to produce intermediate-mass seed black holes of 10^3–$10^5\,M_\odot$ onto which further accretion can take place. One picture of black hole seed formation is the direct collapse of gas clouds in the center of minihalos, see [131]. Begelman's [132] 'quasi-stars' offer another route to the formation of SMBHs. Another new idea for explaining the existence of SMBHs has been proposed in [133], where a black hole moving inside of a star cluster can have rapid accretion and become very massive.

Recently, subsequent to our work on supermassive dark stars, there has been renewed interest in supermassive stars (SMSs) of purely gas origin. These resemble SMDSs in many ways and may also serve as explanations of supermassive black holes; see [134–138] for more details. The proposed SMSs, however, require very high accretion rates, $\dot{M} \gtrsim 10^{-1}\,M_\odot$, and hence can only form in atomic-cooling halos like LMH in equation (9). A detailed comparison of the structure and evolution between SMSs and supermassive dark stars will be published elsewhere [115].

As we have seen, SMDSs could form in a variety of halo environments, ending up with different final stellar masses. We described earlier in this review the case of SMH (see equation (8)). Alternatively, in the 'large minihalo case' (LMH) of equation (9), a hydrogen/helium molecular cloud may start to contract in a $10^8\,M_\odot$ halo. Here the virial temperature is sufficiently high for the gas cloud to cool by hydrogen line cooling; then the higher temperature implies a larger accretion rate of $10^{-1}\,M_\odot\ \mathrm{yr}^{-1}$. We studied the growth of SMDSs using both polytropes and MESA for this LMH case. The amount of baryonic mass in these larger halos is $1.5 \times 10^7 M_\odot$, and potentially, all of this mass could go into the SMDS.

Dark stars could provide seeds for the many supermassive BHs seen throughout the Universe and at early times. Once the dark matter fuel inside a dark star is exhausted, then the star contracts to maintain pressure support. Lighter DSs become fusion-powered for $\sim 10^6$ years before collapsing to black holes. On the other end of the spectrum, the most massive supermassive dark stars may collapse directly to supermassive black holes with masses of $>10^5\,M_\odot$ without any fusion phase at all, similar to the monolithic collapse of central gas clouds in the more traditional scenarios of forming supermassive black holes. Either mechanism would clearly help to provide seed BHs that might explain the many SMBHs found throughout the Universe.

8.1. Gamma-ray constraints

γ-rays can constrain the mass and abundance of DSs. A series of papers [139, 140] explored the detection prospects for γ-rays produced in dark matter annihilations in the DM spikes surrounding black holes for a range of star formation scenarios, black hole masses, and dark matter annihilation modes. Here we review the constraints obtained by comparing the γ-rays measured by the FERMI gamma-ray space telescope [141] with the predictions of γ-ray annihilation products from the remnants of early DSs in our Galaxy today (see also [142]). In hierarchical structure formation, smaller halos are incorporated into larger halos. Some of the same halos which hosted the first stars now have merged inside our own Milky Way Galaxy. As a consequence, there may be a large number of remnant BHs inside our Galaxy.

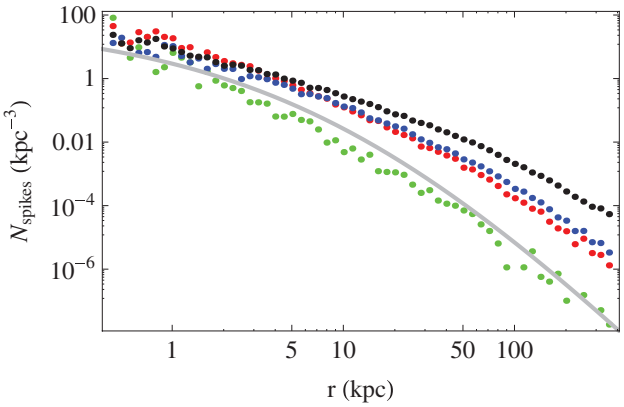

Figure 10. The number density of black hole spikes in the Milky Way as a function of galactic radius for star formation models with early (green), intermediate (red), and late (blue) z_f as described in the text and assuming 100 percent efficiency in dark star formation. Curves have been obtained using the Via Lactea (VL) II N-body simulation. The black points illustrate the total dark matter density profile at $z = 0$ in VL-II; although the normalization of these points is arbitrary, it is useful to illustrate that the total DM profile is more extended than the distribution of black holes with DM spikes. Also shown as a solid grey curve is the analytical fit found in [142, 143]. Our simulations show 409, 7983, and 12 416 DM spikes in the Milky Way for the Early, Intermediate, and Late scenarios, respectively. (Figure taken from [140]. © SISSA Medialab Srl. Reproduced by permission of IOP Publishing. All rights reserved.)

After a DS dies, the remaining BH can still be surrounded by a DM reservoir in the form of a dark matter 'spike'. Annihilation of the DM inside the DS spikes can produce a copious number of γ-rays due to the high DM density. These γ-rays can be detected by FERMI.

Many black holes of mass 10–$10^5\,M_\odot$ that formed at the centers of minihalos survive in the Universe today. Assuming some fraction of high-redshift minihalos which hosted a DS, one can estimate the distribution of their remnant black holes today. Although some of the original minihalos would have merged with other DM halos, resulting in disruption, one can still follow the evolution of the black holes and their DM spikes in simulations. Some of us [139, 140] used the Via Lactea-II N-body simulation of [144] to track black hole spikes from the redshift of their formation to $z = 0$. In this way, the black hole population could be estimated in a galaxy like our Milky Way today.

The number of spikes depends on an important parameter—the range of redshifts during which the first stars can form. Since the redshift at which the increasing UV background and/

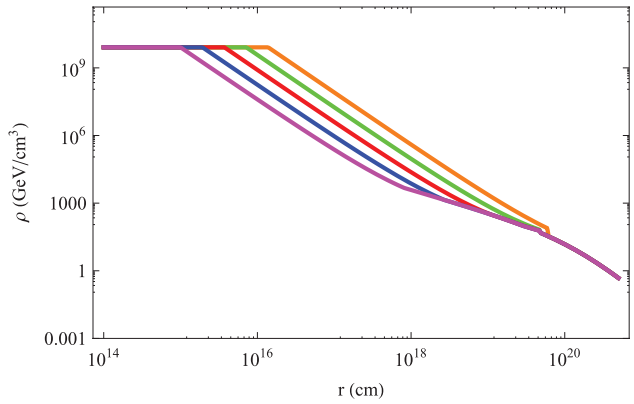

Figure 11. Density profiles for contracted dark matter halos surrounding black holes of mass $10\,M_\odot$ (magenta), $10^2\,M_\odot$ (blue), $10^3\,M_\odot$ (red), $10^4\,M_\odot$ (green), and $10^5\,M_\odot$ (orange), from bottom to top, assuming that the central black hole in each case formed at $z = 15$ in a halo of mass $10^6\,M_\odot$ (Figure taken from [140]. © SISSA Medialab Srl. Reproduced by permission of IOP Publishing. All rights reserved.)

or metal enrichment results in the truncation of first star formation is poorly constrained, three scenarios were examined for the end of first star formation: early ($z_f = 23$), intermediate ($z_f = 15$), and late ($z_f = 11$). Figure 10 illustrates the number density of BH spikes as a function of galactic radius for these three cases. The late scenario has the largest number of spikes.

Figure 11 shows the contracted halo profiles today for DM spikes due to black holes of various masses for the case where the central object formed at $z = 15$. We note that the power law portion of the profile is independent of WIMP mass. In the central regions, closest to the black hole, some of the DM has annihilated away in the time since the formation of the central mass. A more massive dark star will have more adiabatic contraction, which will generate a larger spike, as seen in figure 11. In addition, the DM particle properties will also affect the number of γ-rays produced. For instance, low-mass DM will have a higher annihilation rate compared to a more massive DM particle (for a fixed cross section). Different annihilation channels produce different number of photons. Leptons produce significantly fewer photons compared to gauge mediators and quarks. Hence, a 10 GeV WIMP annihilating into $b\bar{b}$ will produce many more γ-rays compared to a 100 GeV WIMP annihilating into leptons such as $\mu\bar{\mu}$.

The data from FERMI was used in a two-pronged approach to constrain the number of black holes in the Milky Way halo and, consequently, the number of DSs that could have formed at early times. First, the FERMI First Source Catalog [145] was used to find the minimal distance to the nearest DM spike such that it is not brighter than the brightest source observed by FERMI. From the predicted distribution of such spikes in the Milky Way halo, a limit was extracted on the fraction of minihalos in the early Universe to host a black hole (and survive as a DM spike in our galactic halo today). Second, the FERMI measurement of the diffuse γ-ray background was used to constrain the population of DM spikes contributing to the diffuse flux today, thereby setting a second limit on the fraction of minihalos in the early Universe to become DM spikes in our Galactic halo.

These data were used to constrain the efficiency of DS formation $f_{\rm DS}$, i.e. the fraction of early minihalos that contained a DS and their black hole remnants. In figure 12, we show the constraints from point sources and from the diffuse γ-ray background. One can see that the constraints are the strongest for very massive DSs and for annihilation into quarks and gauge bosons. It is important to emphasize that the constraint is for halos which have a mass below $10^7 M_\odot$. If the supermassive DSs form inside halos more massive than $10^7 M_\odot$, the constraints would be much weaker.

9. Dark stars and their impact on reionization and radiation backgrounds

If DSs of various sizes constitute a part of early stellar populations, they will impact the history of reionization, and affect the optical depth of the intergalactic medium as probed by the cosmic microwave background. This allows to constrain the abundance and properties of DSs, albeit the analysis is highly complicated by the fact that reionization models suffer from poorly known astrophysical parameters. Only few studies have been done in the past so far to determine the effects of DSs on reionization, and those were limited to DSs with masses smaller than about 1000 $M_\odot$. We stress that the ionizing photon flux for a given stellar mass falls off very abruptly, as the relative contribution of DM annihilation heating to the star's total energy budget is increased. In order to study the impact on reionization, [31] considers a stellar population of either *only* main-sequence dominated DSs (with some DM capture) or DM-capture-dominated DSs. In neither population is DM heating dominant due to annihilation of adiabatically-contracted DM and DS masses are below about 1000 $M_\odot$. It is found that the former case delays reionization while the latter case hasten it. These results are in accordance with the analysis of [32] in the respective limit cases. However, [32] considers more varied DS lifetimes and DS fractions of the total population which does include Pop III and Pop II stars, as well. Furthermore, another population considered consists of DSs whose fuel is dominated by adiabatically-contracted DM (and no capture), albeit only for a time as long as about 0.3–0.4 Myrs, at which point the DSs have masses of about 800 $M_\odot$. This case corresponds to a DS history akin to the one depicted in figure 2. As we have pointed out above, this case is pessimistic in terms of how long a supply of DM could be sustained. The 'dark star proper' considered in [32] encompasses this case, as well as the transition of this case to phases of meager or extreme DM capture, in which case the lifetime of the DS is extended up to 500 Myrs. We stress that this case does *not* include those SMDSs which are predominantly fueled by the annihilation of adiabatically-contracted DM. DSs dominated by DM heating due to capture are always hotter and denser than those without capture included (see section 5 and figure 3). Therefore, their ionizing UV photon budget will be necessarily higher than that for the case without capture.

[32] find that, in the case where gravity is the only source of DM in the star (i.e. DS without capture), DSs do not affect standard reionization. On the other hand, if dark stars capture

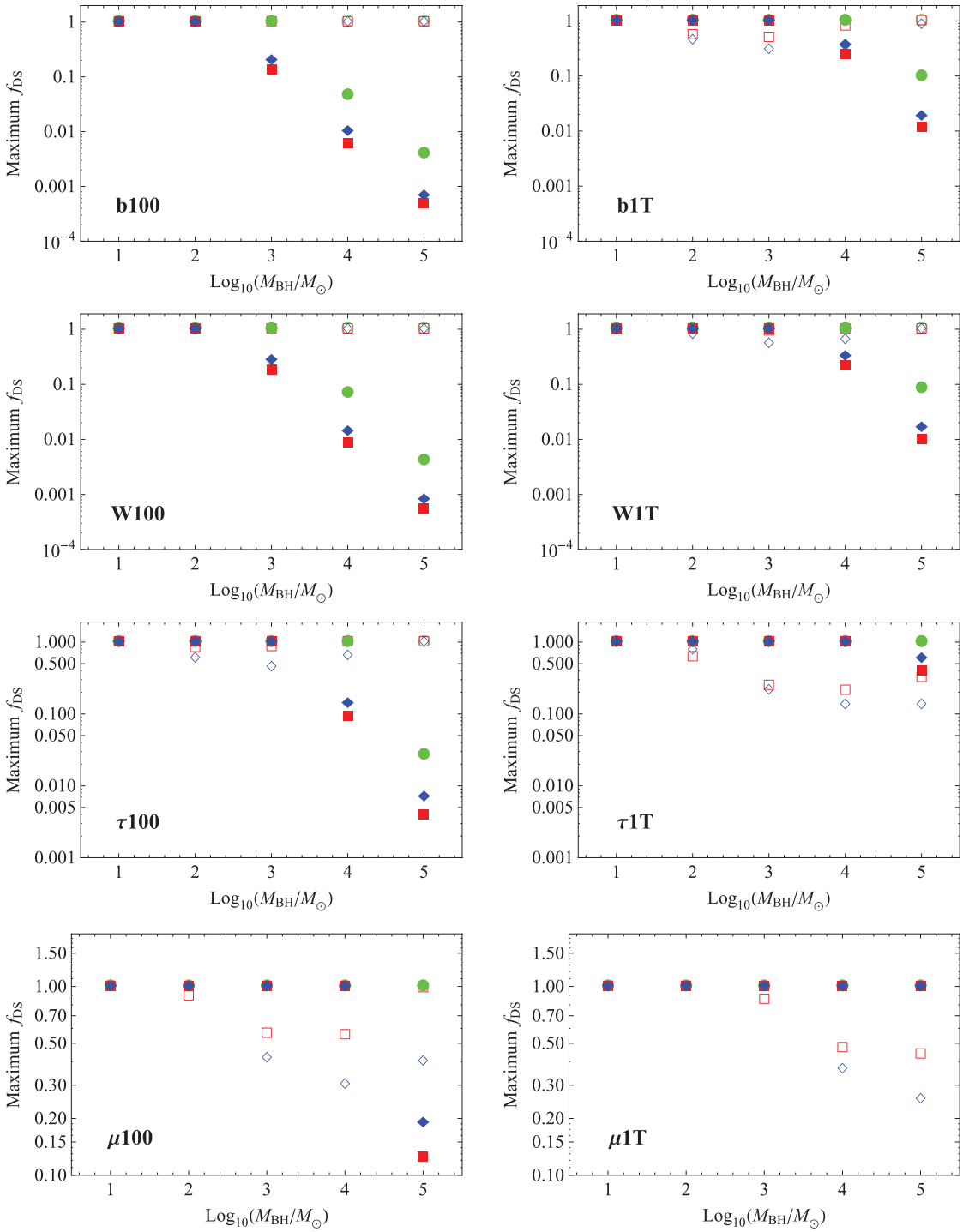

Figure 12. Maximum f_{DS} (fraction of early minihalos which contain a DS) as a function of central black hole mass for the WIMP annihilation into $\tau\bar{\tau}$, W^+W^-, $b\bar{b}$ and $\mu\bar{\mu}$. Green circles, red squares, and blue diamonds are for Early, Intermediate, and Late z_f, respectively. The left panels show $m_\chi = 100$ GeV. The right panels show $m_\chi = 1$ TeV. The solid markers are the limits from point source brightness, while the open markers are from the diffuse γ-ray flux. Each panel assumes a single annihilation channel. Note that the range of f_{DS} displayed differs from panel to panel. (Figure taken from [140]. © SISSA Medialab Srl. Reproduced by permission of IOP Publishing. All rights reserved.)

large amounts of dark matter via nuclear scattering, [32] found that reionization can be substantially delayed, leading to decreases in the integrated optical depth to last scattering and large-scale power in the EE polarization power spectrum. Thus, in principle observations of these quantities from CMB data could be used to bound DS stellar populations. In the intermediate case, where moderate amounts of dark matter are captured by the DS, reionization can instead be sped up slightly, modestly increasing the CMB optical depth. Yet, as pointed out repeatedly in [32], any effect of a DS population on reionization could be degenerate with the effects of the variation of (poorly known) astrophysical parameters, particularly the star formation efficiency and the escape fraction of UV photons out of their halos. Thus, it will be hard

to ascertain whether DSs have a significant impact on the reionization history of the Universe. Still, it may be possible to reconcile certain reionization models and their preferred astrophysical parameters with observations by invoking the idea that some fraction of early stars consists of DSs.

It would be important to re-do some of the previous investigations for the case of supermassive DSs (SMDSs) in the first stellar populations to see how reionization and the associated optical depth may be changed. As of yet, the reionization studies with DSs have only been done for DSs weighing less than 1000 $M_{\odot}$. This is a rich field which warrants more attention for future study.

Another probe of DSs is their impact on the extragalactic background light (EBL), whose main contribution comes from integrated starlight and thermal dust emissions of all cosmic epochs since the formation of the first stars. The EBL consists of the optical to infrared part of the diffuse metagalactic radiation field, and has been identified as a unique probe for the integrated star formation history of the Universe. [146] studied the effect of certain DS models on the EBL and noted that, in comparison to other indirect DM detection signals, the DS-induced component in the EBL is unique in that it is not sensitive to the exact branching ratios of the annihilation yields into photons or charged particles and their resulting spectra, as all annihilation products (except for neutrinos) are trapped and thermalized within the DS. Model atmospheres were calculated in [146] using the PHOENIX code for two DS models from [14], for DS mass 100–1000$M_{\odot}$, with effective surface temperatures between 5000–7500 K (no significant hydrogen ionizing radiation is emitted in this range). For comparison, we showed in figure 6 the SMDS spectra obtained using the TLUSTY stellar atmospheres code for heavier stars of mass $\sim 10^6 M_{\odot}$.

The work of [146] considered the constraints of the EBL on DSs of 100–1000$M_{\odot}$ only. Since the DS formation rate and lifetimes are subject to high uncertainty, a range of possible values was considered. Owing to the lower surface temperatures of DSs in this mass range, the peak in the EBL is shifted towards higher wavelengths (>2 μm), compared to ~ 1 μm for standard Pop III stars of the same mass. By comparing lower and upper limits on the EBL, the authors determined the allowed EBL contribution from DSs in the range of 5–25 nW m^{-2} sr^{-1} for wavelengths between 2 and 10 μm. For example, a DS with 106 $M_{\odot}$, 9×10^6 $L_{\odot}$, a lifetime of 10^8 yrs and a minimum formation redshift of $z = 5$ results in a constraint on the DS formation rate between 5×10^{-4} and 3×10^{-3} yr^{-1} Mpc^{-3}.

It will be interesting to constrain more DS parameters and evolution scenarios in the future, using their contribution to the EBL. As shown in figure 6, the peak wavelength for heavier SMDSs $\sim 10^6 M_{\odot}$ is lower than what was considered by [146], so that the constraints would be quite different.

10. Dark stars existing today

While it is possible for some of the first DM-powered stars to exist today, perhaps in under-dense regions of the Universe where later star formation (with its accompanying ionizing photons) has not yet taken place, a more likely scenario is that later generations of stars may also become DM-powered.

High DM densities are the territories in which dark stars may lurk. DM densities at the center of our galaxy provide a refuge 'safe haven' for dark stars. The dark star menagerie has evolved and diversified. Dark stars today are not the supermassive stars of the past, but instead exist on a much reduced scale compared to their earlier glory due to the lower DM densities found at the galactic center compared to halos at high redshift. Only DSs on the order of a solar mass or less can live on such reduced food supplies. In the Introduction, we already mentioned the earliest references on dark stars in the current Universe.

As with DSs in the early Universe, DSs at the galactic center look a bit different from normal stars unaffected by DM heating. We summarize very briefly the changes made by DM heating on stars at the galactic center; see [38, 47, 48, 50] for more information. Also, [147] studied the effect of DM on stellar clusters, while the use of asteroseismology to detect signatures in the stars produced by the presence of DM has been studied in [148, 149]. We also note that the authors of [50] have written the darkstars code: a publicly available stellar evolution package taking DM heating in stars into account. Let us take as the starting point a hydrogen burning star and examine the changes as DM heating also becomes important. Stars at the galactic center capture DM via scattering. As more DM is captured, DM heating begins to power the star. The negative heat capacity of a star causes it to expand and cool. Fusion becomes less important as the central temperature and density of the star drop. The star can reverse its descent onto the main sequence and instead traverses up the Hayashi track. Figure 13 illustrates the evolutionary tracks of stars of different masses, as WIMPs provide varying fractions of the stars' total energy budgets. DSs at the galactic center observationally would look like young stars. With a sufficient amount of DM heating, fusion shuts off completely. With a limitless supply of DM, the star's life can be extended indefinitely, at least much longer than if powered by fusion. Hence possibly both the first and last stars of the Universe might well be dark stars.

A second breed of DSs dubbed 'WIMP burners' can live off DM as well, see [44, 46]. WIMP burners are degenerate stars (white dwarves or neutron stars). At the galactic center, there is a large number of white dwarves and neutron stars. Many of these stars, which would otherwise become fainter with time, can be warmed up by DM heating. While the rest of stars continue to evolve, white dwarves and neutron stars will appear anomalously hot and young due to the DM heating.

Dark stars at the galactic center are potentially observable. The galactic center despite being nearby is shrouded in dust. In order to observe stars at the galactic center requires going deep into the near infrared, which will be possible with the next generation of telescopes. The thirty-meter telescope TMT, which will turn on in the next few years, can observe stars up to magnitude 22 in the K band which corresponds to stars with sub-solar masses [150]; these could be affected by DM heating. JWST could also detect sub-solar mass stars at the galactic center. If DM affects stars at the galactic center,

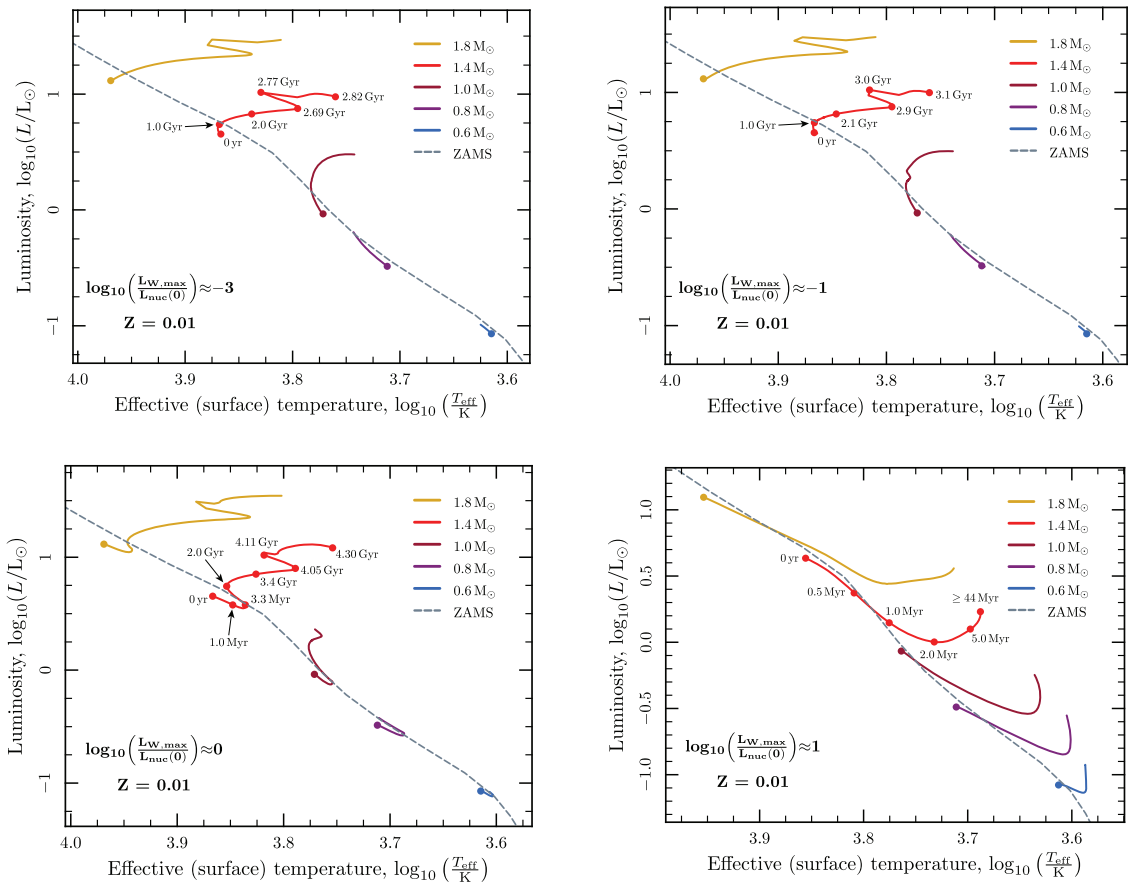

Figure 13. HR diagram showing the evolutionary tracks followed by stars of different masses, as WIMPs are allowed to provide different fractions of the stars' total energy budgets. The energy provided by WIMP annihilation is shown in the bottom left of each sub-plot as the ratio of the maximum luminosity achieved by WIMP annihilation to the initial luminosity due to fusion. Starting points of tracks are indicated with filled, unlabelled circles, whilst labelled circles give indicative ages during the evolution of $1.4M_{\odot}$ stars. Simulations have been halted when the star exhausts its core hydrogen supply or reaches the current age of the Universe. Stars with a greater luminosity contribution from WIMPs push further up the Hayashi track and spend longer there before returning to the main sequence. Those which come to be entirely dominated by WIMP annihilation (*bottom right*) evolve back up the Hayashi track on the thermal timescale and halt, holding their position well beyond the age of the Universe. (Figure taken from [47] with kind permission of authors. Reproduced by permission from Oxford University Press on behalf of the Royal Astronomical Society.)

then the low-mass end of the main sequence would develop a bump as the low-mass stars are pushed up the Hayashi track. The high-mass end of the main sequence will be unaffected by DM heating since the energy generated by DM heating will be small compared to energy generated via fusion. In the case of degenerate stars, white dwarves will also look anomalously hot compared to the age of stars at the galactic center. Hence, the galactic center offers a good hunting ground for DSs.

11. Summary

Dark stars are stars made (almost entirely) of hydrogen and helium but powered by dark matter (DM) annihilation, rather than by fusion. They are in hydrostatic and thermal equilibrium, but with an unusual power source. We discussed dark stars (DSs) throughout the history of the Universe, both at early times and today. Our focus was the dark stars that may be the first stars to form in the Universe. We have reviewed how they come into existence, how they grow as long as dark matter fuel persists, and their stellar structure and evolution. The studies were done in two different ways, first assuming polytropic interiors and more recently using the MESA stellar evolution code; the basic results are the same. The structure and evolution of DSs can be seen in figures 2–5. DSs are giant, puffy (∼10 AU) and cool (surface temperatures ∼10 000 K) objects. They initially weigh about $\sim 1\,M_{\odot}$, and they grow via accretion from the surrounding material. As long as they have DM fuel, their surface temperatures remain cool enough that they can keep growing; they do not produce ionizing photons which prevent further accretion. Some dark stars may grow to be supermassive dark stars, even reaching masses $>10^6\,M_{\odot}$ and luminosities $>10^9\,L_{\odot}$.

It is interesting to speculate that the Initial Mass Function of the first fusion-powered stars may be determined by the details of the dark matter distribution resulting from cosmological structure formation. Individual DSs in different halos may end up with a variety of different masses, depending on the details of the evolution of the halos they live in. Then, the final DS masses determine the initial masses of the standard Population III stars. Once the dark matter fuel inside the DS is

exhausted, then the star contracts to maintain pressure support. Lighter DSs become fusion-powered. On the other end of the spectrum, the most massive dark stars may collapse directly to supermassive black holes (BHs) with masses of $>10^5 M_\odot$ without any fusion phase at all, thereby providing seed BHs for the many supermassive BHs found throughout the Universe. Thus, the initial masses of the first fusion-powered stars may depend on the DM environment within which the earlier DSs grow.

Supermassive dark stars would be detectable in upcoming James Webb Space Telescope (JWST) observations. We have shown their spectra and signatures in JWST. In addition, a new research direction is the study of pulsations in DSs which lead to variability in their light output. Such variability could be used to tackle the question of how one can differentiate a DS from an early galaxy. Initial investigations found a variety of pulsation periods, including some which are of the order of months in the observer's frame. If the pulsations are detectable, DSs may in principle someday be used as novel standard candles for cosmological studies. It will also be possible to learn about or even possibly discover WIMP dark matter by observing the properties of DSs.

We mention briefly an interesting speculation about another way to detect supermassive DSs. Black holes emit gravitational waves when they coalesce in a binary merger. BHs are point masses relative to DSs. If DSs do grow to be quite massive, their mergers should also yield a gravitational wave signature. The fact that they are extended should make their gravitational wave signature distinguishable from that of supermassive BHs of similar masses. Could this be a potentially interesting way to detect DSs with LIGO and maybe with eLISA? Furthermore, they are composed of relatively cool baryons, so the electromagnetic signature of the event should also be possibly quite distinct from that of a much hotter accretion disk.

The idea that a new type of star may be discovered in the near future is very exciting.

Acknowledgments

We would like to thank our collaborators on the papers reviewed in this paper: A Aguirre, P Bodenheimer, J Diemand, P Gondolo, I Iliev, C Ilie, M Montgomery, B Paxton, E Ruiz, P Sandick, J Sellwood, P Shapiro, and D Winget. KF and TRD acknowledge support from the U.S. Department of Energy under grant DOE-FG02-95ER40899 and the Michigan Center for Theoretical Physics at the University of Michigan. MV acknowledges support from the U.S. National Science Foundation via grant AST-0908346. DS and KF are grateful for financial support from the Swedish Research Council (VR) through the Oskar Klein Centre and Stockholm University.

References

[1] Jungman G, Kamionkowski M and Griest K 1996 Supersymmetric dark matter *Phys. Rep.* **267** 195–373
[2] Bertone G, Hooper D and Silk J 2005 Particle dark matter: evidence, candidates and constraints *Phys. Rep.* **405** 279–390
[3] Ade P A R *et al* and Planck Collaboration 2014 Planck 2013 results. XVI. Cosmological parameters *Astron. Astrophys.* **571** A16
[4] Hinshaw G *et al* 2013 Nine-year Wilkinson microwave anisotropy probe (WMAP) observations: cosmological parameter results *Astrophys. J. Suppl. Ser.* **208** 19
[5] Shapiro P R, Iliev I T and Raga A C 2004 Photoevaporation of cosmological minihaloes during reionization *Mon. Not. R. Astron. Soc.* **348** 753–82
[6] Ripamonti E and Abel T 2006 The formation of primordial luminous objects *Joint Evolution of Black Holes and Galaxies* (*Series in High Energy Physics, Cosmology and Gravitation*) ed F Haardt, V Gorini, U Moschella and M Colpi (Abingdon: Taylor & Francis) pp 239–89
[7] Barkana R and Loeb A 2001 In the beginning: the first sources of light and the reionization of the universe *Phys. Rep.* **349** 125–238
[8] Bromm V and Larson R B 2004 The first stars *Ann. Rev. Astron. Astrophys.* **42** 79–118
[9] Yoshida N, Omukai K and Hernquist L 2008 Protostar formation in the early universe *Science* **321** 669
[10] Abel T, Bryan G L and Norman M L 2002 The formation of the first star in the universe *Science* **295** 93
[11] Yoshida N, Omukai K, Hernquist L and Abel T 2006 Formation of primordial stars in a LCDM universe *Astrophys. J.* **652** 6–25
[12] Spolyar D, Freese K and Gondolo P 2008 Dark matter and the first stars: a new phase of stellar evolution *Phys. Rev. Lett.* **100** 051101 (paper I)
[13] Freese K, Bodenheimer P, Spolyar D and Gondolo P 2008 Stellar structure of dark stars: a first phase of stellar evolution resulting from dark matter annihilation *Astrophys. J. Lett.* **685** L101–4
[14] Spolyar D, Bodenheimer P, Freese K and Gondolo P 2009 Dark stars: a new look at the first stars in the universe *Astrophys. J.* **705** 1031–42
[15] Freese K, Ilie C, Spolyar D, Valluri M and Bodenheimer P 2010 Supermassive dark stars: detectable in JWST *Astrophys. J.* **716** 1397–407
[16] Rindler-Daller T, Montgomery M H, Freese K, Winget D E and Paxton B 2015 Dark stars: improved models and first pulsation results *Astrophys. J.* **799** 210
[17] Chandrasekhar S 1939 *An Introduction to the Study of Stellar Structure* (Chicago, IL: The University of Chicago Press)
[18] McKee C F and Tan J C 2008 The Formation of the first stars. II. Radiative feedback processes and implications for the initial mass function *Astrophys. J.* **681** 771–97
[19] Pasham D R, Strohmayer T E and Mushotzky R F 2014 A 400-solar-mass black hole in the galaxy M82 *Nature* **513** 74–6
[20] Mezcua M, Roberts T P, Lobanov A P and Sutton A D 2015 The powerful jet of an off-nuclear intermediate-mass black hole in the spiral galaxy NGC 2276 *Mon. Not. R. Astron. Soc.* **448** 1893–9
[21] Iocco F 2008 Dark matter capture and annihilation over the first stars: preliminary estimates *Astrophys. J.* **677** L1
[22] Iocco F, Bressan A, Ripamonti E, Schneider R, Ferrara A and Marigo P 2008 Dark matter annihilation effects on the first stars *Mon. Not. R. Astron. Soc.* **390** 1655–69
[23] Taoso M, Bertone G, Meynet G and Ekstrom S 2008 Dark matter annihilations in Pop III stars *Phys. Rev.* D **78** 123510
[24] Yoon S-Ch, Iocco F and Akiyama S 2008 Evolution of the first stars with dark matter burning *Astrophys. J.* **688** L1–5
[25] Ripamonti E *et al* 2009 WIMP annihilation effects on primordial star formation *Proc. Sci.* **IDM2008** 075 (arXiv: 0903.0346)
[26] Gondolo P, Huh J-H, Do Him H and Scopel S 2010 Dark matter that can form dark stars *J. Cosmol. Astropart. Phys.* JCAP7(2010)26

[27] Ripamonti E, Iocco F, Ferrara A, Schneider R, Bressan A and Marigo P 2010 First star formation with dark matter annihilation *Mon. Not. R. Astron. Soc.* **406** 2605–15

[28] Sivertsson S and Gondolo P 2011 The WIMP capture process for dark stars in the early universe *Astrophys. J.* **729** 51

[29] Zackrisson E, Scott P, Rydberg C-E, Iocco F, Edvardsson B, Östlin G, Sivertsson S, Zitrin A, Broadhurst T and Gondolo P 2010 Finding high-redshift dark stars with the James Webb Space Telescope *Astrophys. J.* **717** 257–67

[30] Zackrisson E, Scott P, Rydberg C-E, Iocco F, Sivertsson S, Östlin G, Mellema G, Iliev I T and Shapiro P R 2010 Observational constraints on supermassive dark stars *Mon. Not. R. Astron. Soc.* **407** L74–8

[31] Schleicher D R G, Banerjee R and Klessen R S 2009 Dark stars: implications and constraints from cosmic reionization and extragalactic background radiation *Phys. Rev.* D **79** 043510

[32] Scott P, Venkatesan A, Roebber E, Gondolo P, Pierpaoli E and Holder G 2011 Impacts of dark stars on reionization and signatures in the cosmic microwave background *Astrophys. J.* **742** 129

[33] Steigman G, Sarazin C L, Quintana H and Faulkner J 1978 Dynamical interactions and astrophysical effects of stable heavy neutrinos *Astron. J.* **83** 1050–61

[34] Krauss L M, Freese K, Spergel D N and Press W H 1985 Cold dark matter candidates and the solar neutrino problem *Astrophys. J.* **299** 1001

[35] Srednicki M, Olive K A and Silk J 1987 High-energy neutrinos from the sun and cold dark matter *Nucl. Phys.* B **279** 804–23

[36] Freese K 1986 Can scalar neutrinos or massive Dirac neutrinos be the missing mass? *Phys. Lett.* B **167** 295–300

[37] Krauss L M, Srednicki M and Wilczek F 1986 Solar system constraints and signatures for dark matter candidates *Phys. Rev.* D **33** 2079–83 (Revised version of NSF-ITP-85-58)

[38] Salati P and Silk J 1989 A stellar probe of dark matter annihilation in galactic nuclei *Astrophys. J.* **338** 24–31

[39] Bouquet A and Salati P 1989 Dark matter and the suppression of stellar core convection *Astrophys. J.* **346** 284–8

[40] Faulkner J and Gilliland R L 1985 Weakly interacting, massive particles and the solar neutrino flux *Astrophys. J.* **299** 994–1000

[41] Spergel D N and Press W H 1985 Effect of hypothetical, weakly interacting, massive particles on energy transport in the solar interior *Astrophys. J.* **294** 663–73

[42] Aartsen M G *et al* 2013 Search for dark matter annihilations in the Sun with the 79-string IceCube detector *Phys. Rev. Lett.* **110** 131302

[43] Bouquet A and Salati P 1989 Life and death of cosmions in stars *Astron. Astrophys.* **217** 270–82

[44] Moskalenko I V and Wai L L 2007 Dark matter burners *Astrophys. J. Lett.* **659** L29–32

[45] Scott P C, Edsjö J and Fairbairn M 2008 Low mass stellar evolution with WIMP capture and annihilation *Dark Matter in Astroparticle and Particle Physics* ed H V Klapdor-Kleingrothaus and G F Lewis (Singapore: World Scientific) pp 387–92

[46] Bertone G and Fairbairn M 2008 Compact stars as dark matter probes *Phys. Rev.* D **77** 043515

[47] Scott P, Fairbairn M and Edsjö J 2009 Dark stars at the Galactic centre—the main sequence *Mon. Not. R. Astron. Soc.* **394** 82–104

[48] Casanellas J and Lopes I 2009 The formation and evolution of young low-mass stars within halos with high concentration of dark matter particles *Astrophys. J.* **705** 135–43

[49] Hooper D, Spolyar D, Vallinotto A and Gnedin N Y 2010 Inelastic dark matter as an efficient fuel for compact stars *Phys. Rev.* D **81** 103531

[50] Scott P, Edjsö J and Fairbairn M 2010 The darkstars code:. a publicly available dark stellar evolution package *Dark Matter in Astrophysics and Particle Physics, Dark 2009* ed H V Klapdor-Kleingrothaus and I V Krivosheina (Singapore: World Scientific) pp 320–7

[51] Hooper D and Goodenough L 2011 Dark matter annihilation in the Galactic center as seen by the Fermi gamma ray space telescope *Phys. Lett.* B **697** 412–28

[52] Drlica-Wagner A and for the Fermi LAT Collaboration 2012 Constraints on dark matter and supersymmetry from LAT observations of dwarf galaxies arXiv: 1210.5558

[53] Barwick S W *et al* 1997 Measurements of the cosmic ray positron fraction from 1 GeV to 50 GeV *Astrophys. J.* **482** L191–4

[54] Adriani O *et al* 2013 Cosmic-ray positron energy spectrum measured by PAMELA *Phys. Rev. Lett.* **111** 081102

[55] Corti C 2014 The cosmic ray electron and positron spectra measured by AMS-02 arXiv: 1402.0437

[56] Accardo L *et al* 2014 High statistics measurement of the positron fraction in primary cosmic rays of 0.5–500 GeV with the alpha magnetic spectrometer on the international space station *Phys. Rev. Lett.* **113** 121101

[57] Lopez A, Savage C, Spolyar D and Adams D Q 2016 Fermi/LAT observations of dwarf galaxies highly constrain a dark matter interpretation of excess positrons seen in AMS-02, HEAT, and PAMELA *J. Cosmol. Astropart. Phys.* JCAP03(2016)033

[58] Adam R *et al* and Planck Collaboration 2015 Planck 2015 results. I. Overview of products and scientific results arXiv: 1502.01582

[59] Natarajan A, Tan J C and O'Shea B W 2009 Dark matter annihilation and primordial star formation *Astrophys. J.* **692** 574–83

[60] Freese K, Gondolo P, Sellwood J A and Spolyar D 2009 Dark matter densities during the formation of the first stars and in dark stars *Astrophys. J.* **693** 1563–9

[61] Freese K, Spolyar D and Aguirre A 2008 Dark matter capture in the first stars: a power source and limit on stellar mass *J. Cosmol. Astropart. Phys.* JCAP11(2008)14

[62] Navarro J F, Frenk C S and White S D M 1996 The structure of cold dark matter halos *Astrophys. J.* **462** 563–75

[63] Brooks A M and Zolotov A 2014 Why baryons matter: the kinematics of dwarf spheroidal satellites *Astrophys. J.* **786** 87

[64] Ripamonti E, Mapelli M and Ferrara A 2007 The impact of dark matter decays and annihilations on the formation of the first structures *Mon. Not. R. Astron. Soc.* **375** 1399–408

[65] Gondolo P, Edsjö J, Ullio P, Bergström L, Schelke M and Baltz E A 2004 DarkSUSY: computing supersymmetric dark matter properties numerically *J. Cosmol. Astropart. Phys.* JCAP7(2004)8

[66] Fornengo N, Pieri L and Scopel S 2004 Neutralino annihilation into γ rays in the Milky way and in external galaxies *Phys. Rev.* D **70** 103529

[67] Yao W-M *et al* 2006 Review of particle physics *J. Phys. G: Nucl. Phys.* **33** 1–1232

[68] Rossi B 1952 *High-Energy Particles* (Englewood Cliffs, NJ: Prentice-Hall)

[69] Hollenbach D and McKee C F 1979 Molecule formation and infrared emission in fast interstellar shocks. I. Physical processes *Astrophys. J. Suppl. Ser.* **41** 555–92

[70] Yoshida N, Freese K, Gondolo P and Spolyar D in preparation

[71] Gao L, Yoshida N, Abel T, Frenk C S, Jenkins A and Springel V 2007 The first generation of stars in the Λ cold dark matter cosmology *Mon. Not. R. Astron. Soc.* **378** 449–68

[72] Freese K *et al* 2008 Dark stars: dark matter in the first stars leads to a new phase of stellar evolution *IAU Symp.* vol **255** p 56

[73] Iglesias C A and Rogers F J 1996 Updated opal opacities *Astrophys. J.* **464** 943

[74] Lenzuni P, Chernoff D F and Salpeter E E 1991 Rosseland and Planck mean opacities of a zero-metallicity gas *Astrophys. J. Suppl. Ser.* **76** 759–801

[75] Paxton B, Bildsten L, Dotter A, Herwig F, Lesaffre P and Timmes F 2011 Modules for experiments in stellar astrophysics (MESA) *Astrophys. J. Suppl. Ser.* **192** 3

[76] Paxton B *et al* 2013 Modules for experiments in stellar astrophysics (MESA): planets, oscillations, rotation, and massive stars *Astrophys. J. Suppl. Ser.* **208** 4

[77] Bahcall J N 1989 *Neutrino Astrophysics* (New York: Cambridge University Press)

[78] Kippenhahn R and Weigert A 1990 *Stellar Structure and Evolution* (New York: Springer) p 192

[79] Diemand J, Kuhlen M and Madau P 2007 Formation and evolution of galaxy dark matter halos and their substructure *Astrophys. J.* **667** 859

[80] Springel V, Wang J, Vogelsberger M, Ludlow A, Jenkins A, Helmi A, Navarro J F, Frenk C S and White S D M 2008 The aquarius project: the subhaloes of galactic haloes *Mon. Not. R. Astron. Soc.* **391** 1685–711

[81] Klypin A A, Trujillo-Gomez S and Primack J 2011 Dark matter halos in the standard cosmological model: results from the Bolshoi simulation *Astrophys. J.* **740** 102

[82] Blumenthal G R, Faber S M, Flores R and Primack J R 1986 Contraction of dark matter galactic halos due to Baryonic infall *Astrophys. J.* **301** 27

[83] Barnes J and White S D M 1984 The response of a spheroid to a disc field or were bulges ever ellipticals? *Mon. Not. R. Astron. Soc.* **211** 753–65

[84] Ryden B S and Gunn J E 1987 Galaxy formation by gravitational collapse *Astrophys. J.* **318** 15–31

[85] Binney J and Tremaine S 2008 *Galactic Dynamics* 2nd edn (Princeton, NJ: Princeton University Press)

[86] Bardeen J M, Bond J R, Kaiser N and Szalay A S 1986 The statistics of peaks of Gaussian random fields *Astrophys. J.* **304** 15–61

[87] Dubinski J and Carlberg R G 1991 The structure of cold dark matter halos *Astrophys. J.* **378** 496–503

[88] Jing Y P and Suto Y 2002 Triaxial modeling of halo density profiles with high-resolution N-body simulations *Astrophys. J.* **574** 538–53

[89] Bailin J and Steinmetz M 2005 Internal and external alignment of the shapes and angular momenta of ΛCDM halos *Astrophys. J.* **627** 647–65

[90] Allgood B, Flores R A, Primack J R, Kravtsov A V, Wechsler R H, Faltenbacher A and Bullock J S 2006 The shape of dark matter haloes: dependence on mass, redshift, radius and formation *Mon. Not. R. Astron. Soc.* **367** 1781–96

[91] Schwarzschild M 1979 A numerical model for a triaxial stellar system in dynamical equilibrium *Astrophys. J.* **232** 236–47

[92] Goodman J and Schwarzschild M 1981 Semistochastic orbits in a triaxial potential *Astrophys. J.* **245** 1087–93

[93] Gerhard O E and Binney J 1985 Triaxial galaxies containing massive black holes or central density cusps *Mon. Not. R. Astron. Soc.* **216** 467–502

[94] de Zeeuw T 1985 Elliptical galaxies with separable potentials *Mon. Not. R. Astron. Soc.* **216** 273–334

[95] Schwarzschild M 1993 Self-consistent models for galactic halos *Astrophys. J.* **409** 563–77

[96] Merritt D and Fridman T 1996 Triaxial galaxies with cusps *Astrophys. J.* **460** 136

[97] Merritt D and Valluri M 1996 Chaos and mixing in triaxial stellar systems *Astrophys. J.* **471** 82

[98] Dubinski J 1994 The effect of dissipation on the shapes of dark halos *Astrophys. J.* **431** 617–24

[99] Kazantzidis S, Kravtsov A V, Zentner A R, Allgood B, Nagai D and Moore B 2004 The effect of gas cooling on the shapes of dark matter halos *Astrophys. J. Lett.* **611** L73–6

[100] Debattista V P, Moore B, Quinn T, Kazantzidis S, Maas R, Mayer L, Read J and Stadel J 2008 The causes of halo shape changes induced by cooling baryons: disks versus substructures *Astrophys. J.* **681** 1076–88

[101] Valluri M, Debattista V P, Quinn T and Moore B 2010 The orbital evolution induced by baryonic condensation in triaxial haloes *Mon. Not. R. Astron. Soc.* **403** 525–44

[102] Valluri M, Debattista V P, Quinn T R, Roškar R and Wadsley J 2012 Probing the shape and history of the Milky Way halo with orbital spectral analysis *Mon. Not. R. Astron. Soc.* **419** 1951–69

[103] Laskar J 1990 The chaotic motion of the solar system—a numerical estimate of the size of the chaotic zones *Icarus* **88** 266–91

[104] Valluri M and Merritt D 1998 Regular and chaotic dynamics of triaxial stellar systems *Astrophys. J.* **506** 686–711

[105] Valluri M, Debattista V P, Stinson G S, Bailin J, Quinn T R, Couchman H M P and Wadsley J 2013 Halo orbits in cosmological disk galaxies: tracers of formation history *Astrophys. J.* **767** 93

[106] Stinson G S, Bailin J, Couchman H, Wadsley J, Shen S, Nickerson S, Brook C and Quinn T 2010 Cosmological galaxy formation simulations using smoothed particle hydrodynamics *Mon. Not. R. Astron. Soc.* **408** 812–26

[107] Orin Harris 2014 Pico: search for dark matter with bubble chambers http://cosmo2014.uchicago.edu/depot/talk-harris-orin.pdf

[108] Archambault S *et al* 2012 Constraints on low-mass WIMP interactions on ^{19}F from PICASSO *Phys.Lett.* B **711** 153–61

[109] Aprile E *et al* 2013 Limits on spin-dependent WIMP-nucleon cross sections from 225 live days of XENON100 data *Phys. Rev. Lett.* **111** 021301

[110] Agnese R *et al* 2014 Search for low-mass weakly interacting massive particles using voltage-assisted calorimetric ionization detection in the superCDMS experiment *Phys. Rev. Lett.* **112** 041302

[111] LUX Collaboration 2014 First results from the LUX dark matter experiment at the sanford underground research facility *Phys. Rev. Lett.* **112** 091303

[112] Haisch U, Kahlhoefer F and Unwin J 2013 The impact of heavy-quark loops on LHC dark matter searches *J. High Energy Phys.* JHEP07(2013)125

[113] Fox P J, Harnik R, Kopp J and Tsai Y 2012 Missing energy signatures of dark matter at the LHC *Phys. Rev.* D **85** 056011

[114] Hoyle F and Fowler W A 1963 On the nature of strong radio sources *Mon. Not. R. Astron. Soc.* **125** 169

[115] Rindler-Daller T and Freese K 2016 *Mon. Not. R. Astron. Soc.* in preparation

[116] Gondolo P, Freese K, Spolyar D and Bodenheimer P 2013 Numerical evidence for dark star formation: a comment on 'Weakly interacting massive particle dark matter and first stars: suppression of fragmentation in primordial star formation' by Smith *et al* 2012 *Astrophys. J.* **761** 154 (arXiv:1304.7415)

[117] Smith R J, Iocco F, Glover S C O, Schleicher D R G, Klessen R S, Hirano S and Yoshida N 2012 Weakly interacting massive particle dark matter and first stars: suppression of fragmentation in primordial star formation *Astrophys. J.* **761** 154

[118] Stacy A, Pawlik A H, Bromm V and Loeb A 2014 The mutual interaction between Population III stars and self-annihilating dark matter *Mon. Not. R. Astron. Soc.* **441** 822–36

[119] Stacy A, Greif T H and Bromm V 2010 The first stars: formation of binaries and small multiple systems *Mon. Not. R. Astron. Soc.* **403** 45–60

[120] Clark P C, Glover S C O, Klessen R S and Bromm V 2011 Gravitational fragmentation in turbulent primordial gas and the initial mass function of population III stars *Astrophys. J.* **727** 110

[121] Greif T H, Bromm V, Clark P C, Glover S C O, Smith R J, Klessen R S, Yoshida N and Springel V 2012 Formation and evolution of primordial protostellar systems *Mon. Not. R. Astron. Soc.* **424** 399–415

[122] Ilie C, Freese K, Valluri M, Iliev I T and Shapiro P R 2012 Observing supermassive dark stars with James Webb Space Telescope *Mon. Not. R. Astron. Soc.* **422** 2164–86

[123] Freese K, Ruiz E, Valluri M, Ilie C, Spolyar D and Bodenheimer P 2010 Supermassive dark stars: detectable by JWST and HST *AIP Conf. Proc* **1294** 45

[124] Bouwens R J, Illingworth G D, Oesch P A, Trenti M, Stiavelli M, Carollo C M, Franx M, van Dokkum P G, Labbé I and Magee D 2010 Very blue UV-continuum slope β of low luminosity $z \sim 7$ galaxies from WFC3/IR: evidence for extremely low metallicities? *Astrophys. J. Lett.* **708** L69–73

[125] Bouwens R J, Illingworth G D, Labbe I, Oesch P A, Trenti M, Carollo C M, van Dokkum P G, Franx M, Stiavelli M, González V, Magee D and Bradley L 2011 A candidate redshift $z \sim 10$ galaxy and rapid changes in that population at an age of 500Myr *Nature* **469** 504–7

[126] Oesch P A, Bouwens R J, Illingworth G D, Labbé I, Trenti M, Gonzalez V, Carollo C M, Franx M, van Dokkum P G and Magee D 2012 Expanded search for $z \sim 10$ galaxies from HUDF09, ERS, and CANDELS data: evidence for accelerated evolution at $z \gtrsim 8$? *Astrophys. J.* **745** 110

[127] Hubeny I 1988 A computer program for calculating non-LTE model stellar atmospheres *Comput. Phys. Commun.* **52** 103–32

[128] Fan X *et al* 2001 High-redshift quasars found in sloan digital sky survey commissioning data. 3. A color selected sample *Astron. J.* **121** 31

[129] Wu X-B *et al* 2015 An ultraluminous quasar with a twelve-billion-solar-mass black hole at redshift 6.30 *Nature* **518** 512–5

[130] Kormendy J and Ho L C 2013 Coevolution (or not) of supermassive black holes and host galaxies *Ann. Rev. Astron. Astrophys.* **51** 511–653

[131] Loeb A and Rasio F A 1994 Collapse of primordial gas clouds and the formation of quasar black holes *Astrophys. J.* **432** 52–61

[132] Begelman M C 2010 Evolution of supermassive stars as a pathway to black hole formation *Mon. Not. R. Astron. Soc.* **402** 673–81

[133] Alexander T and Natarajan P 2014 Rapid growth of seed black holes in the early universe by supra-exponential accretion *Science* **345** 1330–3

[134] Reisswig C *et al* 2013 Formation and Coalescence of Cosmological Supermassive Black Hole Binaries in Supermassive Star Collapse *Phys. Rev. Lett.* **111** 151101

[135] Montero P J, Janka H-T and Müller E 2012 Relativistic collapse and explosion of rotating supermassive stars with thermonuclear effects *Astrophys. J.* **749** 37

[136] Chen K-J *et al* 2014 General relativistic instability supernova of a supermassive population III star *Astrophys. J.* **790** 162

[137] Whalen D J, Even W, Smidt J, Heger A, Chen K-J, Fryer C L, Stiavelli M, Xu H and Joggerst C C 2013 Supermassive population III supernovae and the birth of the first quasars *Astrophys. J.* **778** 17

[138] Hosokawa T, Yorke H W, Inayoshi K, Omukai K and Yoshida N 2013 Formation of primordial supermassive stars by rapid mass accretion *Astrophys. J.* **778** 178

[139] Sandick P, Diemand J, Freese K and Spolyar D 2012 Gamma-ray constraints on the first stars from annihilation of light WIMPs *Phys. Rev.* D **85** 083519

[140] Sandick P, Diemand J, Freese K and Spolyar D 2011 Black holes in our galactic halo: compatibility with FGST and PAMELA data and constraints on the first stars *J. Cosmol. Astropart. Phys.* JCAP01(2011)018

[141] Ackermann M *et al* 2014 Dark matter constraints from observations of 25 Milky Way satellite galaxies with the Fermi large area telescope *Phys. Rev.* D **89** 042001

[142] Bertone G, Zentner A R and Silk J 2005 A new signature of dark matter annihilations: gamma-rays from intermediate-mass black holes *Phys. Rev.* D **72** 103517

[143] Taoso M, Ando S, Bertone G and Profumo S 2009 Angular correlations in the cosmic gamma-ray background from dark matter annihilation around intermediate-mass black holes *Phys. Rev.* D **79** 043521

[144] Diemand J, Kuhlen M, Madau P, Zemp M, Moore B, Potter D and Stadel J 2008 Clumps and streams in the local dark matter distribution *Nature* **454** 735–8

[145] Abdo A A *et al* 2010 Fermi large area telescope first source catalog *Astrophys. J. Suppl. Ser.* **188** 405–36

[146] Maurer A, Raue M, Kneiske T, Horns D, Elsässer D and Hauschildt P H 2012 Dark matter powered stars: constraints from the extragalactic background light *Astrophys. J.* **745** 166

[147] Casanellas J and Lopes I 2011 Signatures of dark matter burning in nuclear star clusters *Astrophys. J. Lett.* **733** L51

[148] Casanellas J and Lopes I 2011 Towards the use of asteroseismology to investigate the nature of dark matter *Mon. Not. R. Astron. Soc.* **410** 535–40

[149] Casanellas J and Lopes I 2013 First asteroseismic limits on the nature of dark matter *Astrophys. J. Lett.* **765** L21

[150] Weinberg N N, Milosavljević M and Ghez A M 2005 Stellar dynamics at the galactic center with an extremely large telescope *Astrophys. J.* **622** 878